Small fluorescence-activating and absorption-shifting tag for tunable protein imaging in vivo

Marie-Aude Plamont, Emmanuelle Billon-Denis, Sylvie Maurin, Carole Gauron, Frederico M. Pimenta, Christian G. Specht, Jian Shi, Jérôme Quérard, Buyan Pan, Julien Rossignol, et al.

A small fluorescence-activating and absorption-shifting tag for tunable protein imaging in vivo

Marie-Aude Plamont[a,b,c], Emmanuelle Billon-Denis[a,b,c], Sylvie Maurin[a,b,c], Carole Gauron[d], Frederico M. Pimenta[a,b,c], Christian G. Specht[e], Jian Shi[a,b,c], Jérôme Quérard[a,b,c], Buyan Pan[a,b,c], Julien Rossignol[a,b,c], Nelly Morellet[f], Michel Volovitch[d,e], Ewen Lescop[f], Yong Chen[a,b,c], Antoine Triller[e], Sophie Vriz[d,g], Thomas Le Saux[a,b,c], Ludovic Jullien[a,b,c,1] and Arnaud Gautier[a,b,c,1]

[a] École Normale Supérieure – PSL Research University, Department of Chemistry, 24 rue Lhomond, F-75005 Paris, France.

[b] Sorbonne Universités, UPMC Univ Paris 06, UMR 8640 PASTEUR, F-75005 Paris, France.

[c] CNRS, UMR 8640 PASTEUR, F-75005 Paris, France.

[d] Centre for Interdisciplinary Research in Biology (CIRB) CNRS UMR 7241 / INSERM U1050 / Labex MemoLife, PSL Research University / Collège de France, Paris, France.

[e] École Normale Supérieure, Institute of Biology at the Ecole Normale Supérieure (IBENS), CNRS UMR 8197, INSERM U1024, PSL Research University, 46 rue d'Ulm, Paris 75005, France.

[f] Institut de Chimie des Substances Naturelles, CNRS UPR 2301, Université Paris-Saclay, 1 avenue de la Terrasse, 91198 Gif-sur-Yvette, France.

[g] Université Paris Diderot Sorbonne Paris Cité, Paris, France.

[1] To whom correspondence should be addressed.

Arnaud Gautier

École Normale Supérieure, Department of Chemistry

24 rue Lhomond, FR-75005 Paris, France

Telephone: 0033 (0)1 44 32 24 23, E-mail: arnaud.gautier@ens.fr

Ludovic Jullien

École Normale Supérieure, Department of Chemistry

24 rue Lhomond, FR-75005 Paris, France

Telephone: 0033 (0)1 44 32 33 33, E-mail: ludovic.jullien@ens.fr

Classification: Physical Sciences/Chemistry; Biological Sciences/Cell Biology.

Keywords: Fluorescence imaging – Fluorogenic ligand – Directed evolution.

ABSTRACT

This paper presents Y-FAST (Yellow Fluorescence-Activating and absorption-Shifting Tag), a small monomeric protein tag, half as large as the green fluorescent protein (GFP), enabling to fluorescently label proteins in a reversible and specific manner through the reversible binding and activation of a cell-permeant and non-toxic fluorogenic ligand (a so-called fluorogen). A unique fluorogen activation mechanism based on two spectroscopic changes, increase of fluorescence quantum yield and absorption red shift, provides high labeling selectivity. Y-FAST was engineered from the 14-kDa photoactive yellow protein (PYP) by directed evolution using yeast display and fluorescence-activated cell sorting (FACS). Y-FAST is as bright as common fluorescent proteins, exhibits good photostability and allows the efficient labeling of proteins in various organelles and hosts. Upon fluorogen binding, fluorescence appears instantaneously allowing to monitor rapid processes in near real-time. Y-FAST distinguishes itself from other tagging systems because the fluorogen binding is highly dynamic and fully reversible, which enables to rapidly label and unlabel proteins by addition and withdrawal of the fluorogen, opening new exciting perspectives for the development of multiplexing imaging protocols based on sequential labeling.

SIGNIFICANCE

We developed a small protein tag enabling fluorescent labeling of proteins in living cells and in multicellular organisms through the specific binding and activation of a cell-permeant and non-toxic fluorogenic ligand. This tag called Y-FAST was engineered by directed evolution from the Photoactive Yellow Protein (PYP). Y-FAST distinguishes itself from other labeling methods because the fluorogen binding is highly dynamic and fully reversible. Apart from providing new opportunities in super-resolution imaging and biosensor design, this feature enables to rapidly switch on and off the fluorescence of a fusion protein by addition or withdrawing of the fluorogenic ligand, opening exciting ways to perform sequential multiplexing imaging.

\body

INTRODUCTION

Deciphering the complex mechanisms controlling cells and organisms requires effective imaging systems and fluorescent probes to observe biomolecules in real time with high spatiotemporal resolution. Ideal fluorescent probes should be highly specific for their target, bright, photostable, non-toxic, and as small as possible to avoid perturbing the function of their target. They should also exhibit instantaneous and robust fluorescence, and offer the possibility to tune at will the fluorescence of the system for sophisticated imaging protocols. GFP-like fluorescent proteins have revolutionized cell biology providing an easy way to fluorescently tag any protein of interest with absolute specificity through genetic fusion (1-3). However, an increasing number of studies indicate that they are not always optimal probes, as (i) their size and tendency to oligomerize can lead to dysfunctional fusion proteins (4); (ii) their oxygen-dependent fluorescence precludes their use for anaerobic biology (5); (iii) their long maturation (up to 1 hour) prevents real-time monitoring of rapid processes (6); (iv) they display confounding photophysics like photoswitching, kindling or dark-state conversion, which can complicate the interpretation of some experiments (6, 7).

The importance of fluorescent proteins for bioimaging has motivated biologists and chemists to develop alternative strategies to fluorescently label proteins by taking advantage of the unique behavior of fluorogenic chromophores (8). In these approaches, a protein of interest is fused to a protein tag that binds a fluorogenic ligand (so-called fluorogen) and activates its fluorescence. As the fluorogenic ligand is non-fluorescent by its own and becomes strongly fluorescent only upon binding its cognate tag, unspecific fluorescence background in cells remains minimal even in the presence of an excess of fluorogen, thus ensuring high imaging contrast. Flavin-based fluorescent proteins such as FbFPs (9), iLOV (10) and mini-SOG (11) or bilirubin-binding UnaG (12) have been recently proposed as

alternative to GFP because of their small size and oxygen-independent fluorescence. Biliverdin-based fluorescent proteins (IFP1.4 (13), iRFP (14)) have opened new possibilities for imaging protein in deep tissue and in vivo using infrared excitation. Other interesting developments include labeling strategies relying on protein tags, such as SNAP-tag (15), PYP-tag (16), CRABPII (17) or FAPs (18-21), binding (covalently or non-covalently) an exogenously applied fluorogen. These systems present two main advantages: first, the photophysical properties of exogenous fluorogens can be tailored by molecular engineering; second, their flexibility opens new opportunities for on-demand applications wherein fluorescence is desired only at a specific time or at a given density (22).

Herein we present the development of Y-FAST, a small protein tag enabling fluorescent labeling of proteins in living cells and in multi-cellular organisms. Y-FAST is an engineered variant of the monomeric 14-kDa Photoactive Yellow Protein (PYP) (a blue-light photoreceptor from *Halorhodospira halophila* (23-25)) that we evolved to reversibly bind 4-hydroxybenzylidene-rhodanine (HBR) or 4-hydroxy-3-methylbenzylidene-rhodanine (HMBR), two fluorogens identified in the course of this study (**Fig. 1a**). HBR and HMBR are non-fluorescent by themselves, but they fluoresce yellow light upon blue light excitation when bound to Y-FAST. Y-FAST distinguishes itself from existing labeling systems because the binding is not only specific and instantaneous but also highly dynamic and fully reversible. Fluorescence can thus be rapidly switched on and off simply by addition or withdrawal of the fluorogen, providing an additional degree of control. The fast binding dynamics might moreover decrease the apparent photobleaching rate by continuous renewal of the fluorogen as suggested in previous reports (26). Designing a fluorogen-based reporter characterized by a reversible binding both specific and highly dynamic was however challenging, as the high off-rate necessary for a fast exchange dynamics tends to decrease the affinity required for high selectivity. Thus, to maintain high selectivity, we relied on two

spectroscopic changes for fluorogen activation: first, binding of H(M)BR to Y-FAST results in a significant increase of fluorescence quantum yield, and second it induces large absorption red shift. As Y-FAST is the only species promoting these two spectroscopic changes, free or non-specifically bound fluorogen does not contribute to the fluorescence signal, ensuring high imaging contrast.

RESULTS

Fluorogen design

HBR is easily obtained in one step by in-water condensation of the rhodanine to the para-hydroxybenzaldehyde. It is composed of an electron-donating phenol conjugated to an electron-withdrawing rhodanine (**Fig. 1a**). This push-pull structure is analogous to the GFP chromophore 4-hydroxybenzylidene-5-imidazolinone (HBI) (5), known to deexcite non-radiatively in solution but to relax to the ground state radiatively in the rigid barrel of GFP (27). HBR drew our attention as putative fluorogen for the design of Y-FAST for several reasons. First, HBR is almost fully protonated at physiological pH (its pK_A is 8.4 ± 0.1), and it undergoes a 50 nm absorption red shift upon deprotonation as a result of the stronger electron-donation of the phenolate (**Table 1** and **SI Appendix, Fig. S1a,b**). We therefore anticipated that a protein tag stabilizing deprotonated HBR would exhibit a red-shifted absorption with respect to free HBR in pH 7.4 solutions, enabling discrimination of the free and bound states by their absorption properties. Secondly, HBR fluorescence is highly environment-sensitive. In water, the protonated and deprotonated states of HBR emits at 470 and 545 nm with fluorescence quantum yields of 0.02 % and 0.3 % (**Table 1** and **SI Appendix Fig. S1c**), while in viscous solutions (containing 40 % glycerol) they exhibit six- and three-fold higher brightness, respectively. Taken together these spectroscopic properties allowed us to anticipate that binding of HBR to a well-designed protein tag could provide a

unique fluorogenic effect based on two spectroscopic changes: an absorption red shift through binding-induced deprotonation and a fluorescence quantum yield increase via fluorogen immobilization.

Y-FAST is a variant of the photoactive yellow protein engineered by directed evolution

PYP was chosen as scaffold for the design of Y-FAST for several reasons. First, its para-hydroxycinnamoyl (HC) chromophore – covalently tethered to Cys69 and responsible for its blue-light photosensing properties (23-25) – shares structural features with HBR, suggesting that the binding site of PYP could be engineered to bind HBR selectively and reversibly. Moreover, the binding pocket of PYP accommodates HC in its phenolate deprotonated form (25), providing a platform for designing variants able to stabilize deprotonated HBR and thus obtain absorption red shift upon binding. Finally, wild-type PYP has a proven ability as recombinant protein tag (16, 28) and is a small protein (14 kDa) compared to GFP-like fluorescent proteins (26-30 kDa).

To engineer the binding cavity of PYP, we randomized loops and residues in close proximity with the chromophore pocket by saturation mutagenesis (**SI Appendix, Fig. S2**). By screening yeast surface-displayed libraries by fluorescence activating cell sorting (FACS) (29) in the presence of HBR, we successfully identified 47 clones specifically activating HBR fluorescence (**SI Appendix, Fig. S3**). The selected clones all belonged to the library constructed by randomizing the loop 94-101 that gates the entrance of the binding pocket. The emergence of the consensus sequence WxIPTxxx confirmed convergence of the selection process.

Physico-chemical characterization

The most promising variants were expressed in *E. coli* and purified by affinity chromatography for *in vitro* characterization. Titration experiments relying on fluorescence increase to assay complex formation established that all selected variants bound HBR with 0.5-1 µM affinities (**SI Appendix, Table S1** and **Fig. S4**, see **Text S1** for the thermodynamic analysis). When bound to Y-FAST, the best variant of our selection, HBR fluoresces at ~ 530 nm three orders of magnitude more than in solution, and absorbed maximally at ~ 470 nm instead of ~ 400 nm in pH 7.4 solutions, in accordance with HBR being deprotonated when bound (**Table 1** and **SI Appendix, Fig. S5**).

Y-FAST:HBR complex was shown to form extremely rapidly. Addition of HBR to Y-FAST solutions instantaneously produced yellow fluorescence (**Movie S1**). The on- and off-rate kinetic constants were further determined by stopped-flow experiments (**Table 1,** see **SI Appendix, Text S1, Fig. S6** and **Tables S2-S3** for the kinetic analysis). This kinetic analysis indicated that, when [HBR] = K_D, the relaxation time of binding at 25°C was 30 ms. The analysis demonstrated moreover that the binding was not only rapid but also highly dynamic, since the residence time (reciprocal of the off-rate constant) of HBR in the bound state was only 60 ms at 25°C.

Finally, Y-FAST was proved to exist as a monomer in solution up to millimolar concentrations by determining its apparent size by analytical size-exclusion chromatography (**SI Appendix, Fig. S7**) and by measuring its global tumbling correlation time and translational diffusion coefficient using nuclear magnetic resonance (NMR) spectroscopy (see **SI Appendix, Text S2** and **Table S4**). These latter NMR experiments showed in particular that the diffusion coefficient of Y-FAST at 20°C was 1.1×10^{-10} $m^2.s^{-1}$ in perfect agreement with values reported for monomeric wild-type PYP (30), which corresponds to a hydrodynamic radius of 1.9 nm (see **SI Appendix, Text S2** and **Table S4**).

Brightness optimization

The complex between HBR and Y-FAST displays a fluorescence quantum yield of 9 % and a brightness of 4,000 $M^{-1}cm^{-1}$ (**Table 1**). In order to improve its brightness properties, we screened HBR analogs for enhanced fluorescence performance (**SI Appendix, Fig. S8**). We found that HMBR, an analog bearing an additional methyl group on the aromatic ring (**Fig. 1a**), formed a complex with Y-FAST fivefold tighter (**Table 1** and **SI Appendix, Fig. S9**) and fourfold brighter (**Table 1** and **SI Appendix, Fig. S10a,b**). The complex Y-FAST:HMBR (i) exhibits a fluorescence quantum yield of 33 % and an absorption coefficient of 45,000 $M^{-1}cm^{-1}$ (**Table 1**), attaining the fluorescence performance of common fluorescent proteins (1), and (ii) still displays a red-shifted absorption (**Table 1** and **SI Appendix, Fig. S10c**), in agreement with HMBR being deprotonated in the complex (pK_A 8.7 ± 0.1, see **SI Appendix, Fig. S11**). Kinetic analysis revealed that, despite the gain in affinity, the binding remained both fast (the relaxation time is 70 ms at 25 °C when [HMBR] = K_D) and highly dynamic (the residence time of HMBR is 160 ms at 25 °C) (**Table 1,** see also **SI Appendix, Text S1, Fig. S6** and **Tables S2-S3**).

Specific and efficient labeling of fusion proteins in various cellular systems

The labeling selectivity and efficiency was studied in various hosts (bacteria, yeast and mammalian cells) by flow cytometry and confocal microscopy (**SI Appendix, Fig. S12** and **Table S5**). The analysis concluded that HBR and HMBR (i) are cell-permeant, (ii) generate no or negligible fluorescence background, and (iii) do not bind PYP, illustrating the high selectivity of Y-FAST labeling in living cells. The analysis also confirmed that HMBR outperformed HBR for fluorescent labeling of Y-FAST in living cells. Moreover, when labeled with HMBR, Y-FAST reached brightness and photostability performance comparable with the green fluorescent proteins EGFP (31) and UnaG (12) (**SI Appendix, Fig. S13**).

Finally, no toxic or adverse effects were observed at the fluorogen concentrations typically used for imaging (**SI Appendix, Fig. S14**), suggesting that Y-FAST should enable long-term imaging in mammalian cells.

Specific labeling of fusion proteins in various subcellular locations

Y-FAST labeling was shown to be robust in the biologically relevant pH range 5.5–8 (**SI Appendix, Text S3** and **Fig. S15**), allowing thus to anticipate efficient labeling in most organelles. Labeling of HeLa cells expressing various Y-FAST fusions enabled to visualize proteins in various subcellular locations such as the cytoplasm, the nucleus, the cell membrane, the mitochondria, the Golgi apparatus and the cytoskeleton (**Fig. 1b**). The general applicability of Y-FAST was further demonstrated by visualizing post-synaptic clusters of Gephyrin at inhibitory synapses in dissociated spinal cord neurons, illustrating the ability of Y-FAST to label proteins in more delicate cells and confined cellular compartments (**Fig. 1c**).

Specific labeling of fusion proteins in multicellular organisms

The labeling of Y-FAST was then validated in zebrafish embryo, as model of a multicellular organism. Labeling of zebrafish embryos co-expressing mCherry and Y-FAST at different stages during embryogenesis revealed an expression pattern for Y-FAST indistinguishable from that of mCherry (**Fig. 2** and **SI Appendix, Fig. S16a**), indicating that Y-FAST labeling was highly specific *in vivo*. Evaluation of embryo fitness after prolonged exposure (19 hrs) to HMBR revealed no mortality or developmental anomalies (**SI Appendix, Fig. S16b**), proving that HMBR was non-toxic for zebrafish embryos and suggesting therefore that Y-FAST could enable long-term imaging during embryogenesis.

Real-time monitoring of rapid processes

Most GFP-like fluorescent proteins fail to report on protein synthesis in real-time because the rate of appearance of their fluorescence depends not only on the protein synthesis itself but also on the post-translational formation of their chromophore. To show that the rapid labeling of Y-FAST could be an advantage in this context, we followed the cell-free expression of a fusion between mCherry and Y-FAST by monitoring their fluorescence emissions simultaneously (**SI Appendix, Fig. S17**). Even though a single protein was synthesized, we observed different rates of appearance for Y-FAST and mCherry fluorescence: while Y-FAST could be already detected as soon as 10 min after the initiation of the protein synthesis, reaching saturation within 90 min, the mCherry signal only started to appear after 50 min and took over 4 hours to reach saturation as a result of the slow maturation of its chromophore (32, 33). In addition, we compared the expression of mCherry-Y-FAST with that of EGFP and Venus (34), reported to mature within 10 and 40 min *in vitro*, respectively (35), the bilirubin-inducible UnaG, and the *Firefly* luciferase, the latter often employed as reporter of protein synthesis. Although the expression of the different proteins was controlled by the same T7 promoter and should therefore occur at the same rate, we observed various rates of luminescence appearance (**SI Appendix, Fig. S17**). Our experiments revealed that Y-FAST clearly outperforms Venus and mCherry to report on protein synthesis in near real-time, and provides kinetic information comparable with *Firefly* luciferase, EGFP and UnaG.

The labeling of Y-FAST is highly tunable

Given that Y-FAST fluorescence directly depends on HMBR concentration, Y-FAST labeling can be controlled on demand. This feature was used to control the density of emitters independently of the protein expression level by tuning the fluorogen concentration (**SI Appendix, Fig. S18**). Titration experiments in cells were in good agreement with the *in vitro*

results, indicating that the concentration of HMBR in the milieu reflected its intracellular level.

Because of its rapid, reversible and highly dynamic labeling, Y-FAST can be rapidly switched on and off by addition and removal of HMBR. Labeling was shown to occur in cells within about ten seconds, in accordance with high cell permeability of HMBR and immediate complex formation (**Fig. 3a,b**). Rapid replacement of the medium with HMBR-free medium led to protein unlabeling on a similar timescale (**Fig. 3a,b**), in accordance with the short residence time of HMBR. Using a microfluidic device and a multifunctional fluidic controller to switch repeatedly between the labeling and washing solutions, ten cycles of labeling and unlabeling could be performed (**Fig. 3a,b** and **Movie S2**).

The ability to rapidly switch Y-FAST on and off was further evaluated in zebrafish embryo. Significant staining was obtained within 20-30 min of incubation with HMBR (**Fig. 3c** and **Movie S3**). Dimensional analysis revealed that this timescale was in good agreement with the cell experiments (**SI Appendix, Text S4**), demonstrating that HMBR was also highly permeant in zebrafish embryo. This latter feature enabled to reverse the labeling by washing away HMBR and to repeat the labeling (**Fig. 3d**).

Y-FAST opens new opportunities for multiplexing imaging

The ability to reverse the labeling allows the observation of spectrally indistinguishable targets using sequential rounds of fluorogenic labeling, imaging and fluorogen removal. To validate this strategy, we expressed Y-FAST (fused to a membrane anchoring sequence) and the photoswitchable fluorescent protein Dronpa (36) (fused to a nuclear localization signal) in mammalian cells. Iterative labeling/unlabeling of Y-FAST combined with on/off photoswitching of Dronpa enabled to image the two proteins sequentially (**Fig. 3e**).

DISCUSSION

Y-FAST is a PYP variant engineered to specifically activate the fluorogenic HMBR through two specific spectroscopic alterations – increase of fluorescence quantum yield and absorption red shift – providing a unique spectroscopic signature that ensures high imaging contrast. Y-FAST is comparable to common fluorescent proteins in terms of brightness and photostability, and is well suited for imaging proteins in various organelles and in a large variety of systems, from mammalian cells (including neurons) to microorganisms (e.g. *E. coli*, *S. cerevisiae*) and zebrafish. Interestingly, Y-FAST is (i) half as large as GFP-like fluorescent proteins, which should ensure minimal functional perturbation within fusion proteins; (ii) fully monomeric up to millimolar concentrations. Note that being monomeric up to millimolar concentrations corresponds to exhibit no driving force for self-association up to an average intermolecular distance of about 10 nm. This latter feature should permit to avoid unexpected oligomerization as encountered in certain cases with GFP-like proteins expressed in dense and compact environments (e.g. membranes) or within multi-module fusions (e.g. biosensors). All together these properties makes Y-FAST a good alternative to GFP-like fluorescent proteins.

Unlike GFP-like fluorescent proteins, which are fully fluorescent only after post-translational formation of their chromophore, Y-FAST is fluorescent as soon as it is folded provided that the fluorogen is present. This feature enabled to follow in near real-time protein synthesis and opens new opportunities for (i) reporting on fast processes such as early promoter activation, (ii) labeling proteins with short lifetimes or (iii) monitoring single translation or folding events in near real-time.

The ability to control the fluorescence level of Y-FAST independently of its expression level (by choosing the concentration of fluorogen) could find interesting applications in quantitative biology (22). One challenge in this field is to detect changes in protein copy

numbers in single cells or within specific compartments in order to understand their phenotypic state. However, protein copy numbers can vary by six orders of magnitude in mammalian cells (37) surpassing the dynamic range of most fluorescence detectors (typically three orders of magnitude). Systems like Y-FAST should allow the quantitative comparison of populations of cells displaying disparate protein copy numbers just by adjusting the concentration of fluorogen.

Y-FAST distinguishes itself from other labeling systems because labeling is fully reversible. This feature provides high tunability and opens new exciting perspectives to obtain multiplexed images for a large number of distinct target species. Indeed, the number of molecular species that can be imaged simultaneously is often limited by the spectral overlap between labels. Even though spectral deconvolution can be used, the number of molecular readouts that can be simultaneously measured in single cells remains limited in most cases to a handful of species. Several strategies have been proposed for multiplexing in fixed cells relying on iterative staining and removal (38-41): a first target is labeled with a first stain and imaged; the label is removed by physical or chemical means, after which a second orthogonal stain can be applied to label a second target, and so on. Even though these multiplexing approaches open very interesting perspectives for imaging several tens of targets in a single cell, they remain limited to the study of fixed, permeabilized cells in which targets are labeled with oligonucleotide- or antibody-based probes. A collection of systems such as Y-FAST could extend this strategy to live cells, particularly when combined with recently developed targeted genome editing techniques (e.g. CRISPR-Cas9 system) (42).

The possibility to control the fluorescence on demand should also facilitate the implementation of FRET measurements. Estimate of FRET signal requires extensive controls to determine the extent of cross-talk between donor and acceptor (43). The ability to perform multiple experiments on the same sample in absence or presence of the fluorogen (and

therefore with and without the contribution of Y-FAST) could improve FRET imaging protocols. Y-FAST could play the acceptor in a pair with CFP or the donor in a pair with mCherry (see **SI Appendix, Text S5** and **Fig. S19** for FRET characterization between Y-FAST and mCherry). The use of Y-FAST as acceptor could in particular permit to easily determine FRET efficiency by measuring the quenching of the donor fluorescence upon addition of the fluorogen, or conversely the decrease in fluorescence quenching by rapid washing of the fluorogen, thus competing with donor recovery after acceptor photobleaching techniques, but with the additional advantage of the reversibility. The small size of Y-FAST is also an advantage for FRET as it enhances the energy transfer efficiency by enabling *a priori* shorter Förster distances than GFP-like fluorescent proteins. FRET detection could further benefit from the ability to control the labeling density of Y-FAST independently of its expression level to set the donor:acceptor stoichiometry within the range of 1:10 to 10:1 in order to ensure detectable FRET signals.

Finally, the fast exchange dynamics of Y-FAST could be advantageously exploited for super-resolution imaging in live cells. As Y-FAST interconverts spontaneously and rapidly at the single molecule level between a dark (unbound) state and a bright (bound) state, it should behave as a blinking fluorophore (44). Fine-tuning of the exchange dynamics could give access to blinking rates adequate for Single-molecule Localization Microscopies (SLM) (41, 45, 46) or Super-resolution Optical Fluctuation Imaging (SOFI) (44, 47).

In conclusion, the strategy developed in this work is generic and may open new routes for the design of smart probes and biosensors. In particular, HMBR belongs to a series of conjugated donor-acceptor compounds exhibiting various photo-physical/chemical behaviors (48) that could facilitate the design of a collection of Fluorescence-Activating and absorption-Shifting Tags (FASTs) covering the whole visible spectrum for various applications in multiplexed bioimaging and biosensing.

MATERIALS AND METHODS

Mammalian cell culture. HEK293 and HeLa cells were cultured in DMEM supplemented with phenol red, Glutamax I, 10 % fetal calf serum and 1 % penicillin-streptomycin at 37 °C within a 5% CO_2 atmosphere. For microscopic imaging, cells were seeded in µDish IBIDI (Biovalley) coated with poly-L-lysine. Cells were transiently transfected using Genejuice (Merck) according to the manufacturer's protocol. Before imaging, cells were washed with PBS and incubated in DMEM without phenol red complemented with HBR or HMBR at the indicated concentration.

Neuron cultures. Cultures of dissociated spinal cord neurons were prepared from Sprague-Dawley rats (at embryonic day 14) as described previously (49). Neurons were maintained in neurobasal medium containing B27, 2 mM glutamax, 5 U/ml penicillin and 5 µg/ml streptomycin at 36°C and 5% CO_2, co-transfected at day *in vitro* DIV15 with Y-FAST-Gephyrin and mCerulean-Gephyrin plasmid DNA using Lipofectamine 2000 (Invitrogen), and used for experiments on DIV17. Neurons were imaged at 35°C in MEM medium without phenol red, containing 33 mM glucose, 20 mM HEPES, 2 mM glutamax, 1 mM sodium pyruvate and B27. HMBR was added by bath application at a final concentration of 10 µM in imaging buffer.

Zebrafish experiments. Zebrafish were maintained and staged according to Westerfield (50). Experiments were performed using the standard Ab wild type strain. The embryos were incubated at 28°C. The animal facility obtained a French agreement from the ministry of agriculture for all the experiments performed in this manuscript (agreement n° C 75-05-12).

mRNA synthesis was performed using the mMESSAGE mMACHINE Transcription Kit (Ambion Inc). Equivalent volume of 100 ng/ml mRNA was injected into one-cell stage embryos. Embryos were allowed to grow in Volvic mineral water until imaging. To evaluate the effect of HMBR on embryogenesis, groups of about 50 embryos were incubated with HMBR solutions at the indicated concentrations from 50 % epiboly to 24 hpf.

Fluorescence analysis. Flow cytometry analyses were performed on an Accuri C6 cytometer (BD Biosciences). Confocal micrographs were acquired on a Zeiss LSM 710 Laser Scanning Microscope equipped with a Plan Apochromat 63×/1.4 NA oil immersion objective. ZEN software was used to collect the data. Images were analyzed with Image J. Spinning-disk confocal micrographs were acquired on a Nikon Eclipse Ti microscope equipped with a 4×/0.15 N.A objective and a coolSnap HQ2/CDDcamera (Princeton Instrument). Metamorph premier 7.6 software (Molecular Devices) was used to collect the data. Live epifluorescence imaging was performed on an inverted Nikon Eclipse Ti microscope with a 100× oil-immersion objective (N.A. 1.49), a 1.5× magnifying lens and a mercury lamp. Images were acquired with an Andor iXon EMCCD camera (image pixel size 107 nm).

The **SI Materials and Methods** in the **SI Appendix** contains the sections **Chemical Synthesis**; **Plasmid constructions**; **Yeast display; Protein expression, purification and characterization; NMR spectroscopy experiments; Cell-free expression; Viability cellular assay; Microfluidics.**

ACKNOWLEDGMENTS

We thank K. D. Wittrup for providing us with the pCTCON2 vector and the EBY100 yeast strain for the yeast display selection, A. Miyawaki for providing us with plasmids for the

expression of UnaG in bacteria and in mammalian cells. We also thank the Flow Cytometry Facility (IFR83) of the University Pierre and Marie Curie (UPMC), and more particularly Annie Munier for her assistance. This work was supported by the Agence National de la Recherche (ANR-09-MNPS-013-01, ANR-11-BSV8-021-01 and ANR-14-CE09-0002-01), the Region Ile-de-France in the framework of C'Nano IdF (C'Nano IdF is the nanoscience competence of Paris Region, supported by CNRS, CEA, MESR and Region Ile-de-France), PSL Research University (project IMRESOV), France BioImaging, the Equipex Morphoscope 2, the ERC advanced research grant "PlasltInhib", program "Investissements d'Avenir" (ANR-10-LABX-54 MEMO LIFE and ANR-11-IDEX-0001-02 PSL* Research University).

SUPPORTING INFORMATION

The supporting information contains **Movies S1-S3** and **SI Appendix**.

REFERENCES

1. Shaner N, Steinbach P, Tsien R (2005) A guide for choosing fluorescent proteins. *Nat Meth* 2:905–909.

2. Chudakov DM, Matz MV, Lukyanov S, Lukyanov KA (2010) Fluorescent Proteins and Their Applications in Imaging Living Cells and Tissues. *Physiol Rev* 90(3):1103–1163.

3. Snapp EL (2009) Fluorescent proteins: a cell biologist's user guide. *Trends Cell Biol* 19(11):649–655.

4. Wiedenmann JR, Oswald F, Nienhaus GU (2009) Fluorescent proteins for live cell imaging: Opportunities, limitations, and challenges. *Iubmb Life* 61(11):1029–1042.

5. Tsien RY (1998) The green fluorescent protein. *Annu Rev Biochem* 67(1):509–544.

6. Remington SJ (2006) Fluorescent proteins: maturation, photochemistry and photophysics. *Curr Opin Struct Biol* 16(6):714–721.

7. Zimmer M (2002) Green Fluorescent Protein (GFP): Applications, Structure, and Related Photophysical Behavior. *Chem Rev* 102(3):759–782.

8. Jullien L, Gautier A (2015) Fluorogen-based reporters for fluorescence imaging: a review. *Methods Appl Fluoresc* 3(4):042007.

9. Drepper T, et al. (2007) Reporter proteins for in vivo fluorescence without oxygen. *Nat Biotechnol* 25(4):443–445.

10. Chapman S, et al. (2008) The photoreversible fluorescent protein iLOV outperforms GFP as a reporter of plant virus infection. *Proc Natl Acad Sci USA* 105(50):20038–20043.

11. Shu X, et al. (2011) A Genetically Encoded Tag for Correlated Light and Electron Microscopy of Intact Cells, Tissues, and Organisms. *PLoS Biol* 9(4):e1001041.

12. Kumagai A, et al. (2013) A Bilirubin-Inducible Fluorescent Protein from Eel Muscle. *Cell* 153(7):1602–1611.

13. Shu X, et al. (2009) Mammalian Expression of Infrared Fluorescent Proteins Engineered from a Bacterial Phytochrome. *Science* 324(5928):804–807.

14. Filonov GS, et al. (2011) Bright and stable near-infrared fluorescent protein for in vivo imaging. *Nat Biotechnol* 29(8):759–763.

15. Lukinavicius G, et al. (2013) A near-infrared fluorophore for live-cell super-resolution microscopy of cellular proteins. *Nat Chem* 5(2):132–139.

16. Hori Y, et al. (2013) Development of Fluorogenic Probes for Quick No-Wash Live-Cell Imaging of Intracellular Proteins. *J Am Chem Soc* 135(33):12360–12365.

17. Yapici I, et al. (2015) "Turn-On" Protein Fluorescence: In Situ Formation of Cyanine Dyes. *J Am Chem Soc* 137(3):1073–1080.

18. Szent-Gyorgyi C, et al. (2008) Fluorogen-activating single-chain antibodies for imaging cell surface proteins. *Nat Biotechnol* 26(2):235–240.

19. Shank NI, Zanotti KJ, Lanni F, Berget PB, Armitage BA (2009) Enhanced Photostability of Genetically Encodable Fluoromodules Based on Fluorogenic Cyanine Dyes and a Promiscuous Protein Partner. *J Am Chem Soc* 131(36):12960–12969.

20. Ozhalici-Unal H, et al. (2008) A rainbow of fluoromodules: A promiscuous scFv protein binds to and activates a diverse set of fluorogenic cyanine dyes. *J Am Chem Soc* 130(38):12620–12621.

21. Telmer CA, et al. (2015) Rapid, Specific, No-wash, Far-red Fluorogen Activation in Subcellular Compartments by Targeted Fluorogen Activating Proteins. *ACS Chem Biol* 10(5):1239–1246.

22. Schwartz SL, et al. (2015) Fluorogen-Activating Proteins Provide Tunable Labeling Densities for Tracking FcεRI Independent of IgE. *ACS Chem Biol* 10(2):539–546.

23. McRee DE, et al. (1989) Crystallographic structure of a photoreceptor protein at 2.4 A resolution. *Proc Nat Acad Sci USA* 86:6533–6537.

24. Baca M, et al. (1994) Complete Chemical Structure of Photoactive Yellow Protein: Novel Thioester-Linked 4-Hydroxycinnamyl Chromophore and Photocycle Chemistry. *Biochemistry* 33(48):14369–14377.

25. Borgstahl G, Williams D, Getzoff ED (1995) 1.4 .ANG. Structure of Photoactive Yellow Protein, a Cytosolic Photoreceptor: Unusual Fold, Active Site, and Chromophore. *Biochemistry* 34(19):6378–6387.

26. Dean KM, Palmer AE (2014) advances in fluorescence labeling strategies for dynamic cellular imaging. *Nat Chem Biol* 10(7):512–523.

27. Weber W, Helms V, McCammon JA, Langhoff PW (1999) Shedding light on the dark and weakly fluorescent states of green fluorescent proteins. *Proc Nat Acad Sci USA* 96(11):6177–6182.

28. Hori Y, Ueno H, Mizukami S, Kikuchi K (2009) Photoactive yellow protein-based protein labeling system with turn-on fluorescence intensity. *J Am Chem Soc* 131(46):16610–16611.

29. Gai SA, Wittrup KD (2007) Yeast surface display for protein engineering and characterization. *Curr Opin Struct Biol* 17(4):467–473.

30. Khan JS, Imamoto Y, Harigai M, Kataoka M, Terazima M (2006) Conformational Changes of PYP Monitored by Diffusion Coefficient: Effect of N-Terminal α-Helices. *Biophys J* 90(10):3686–3693.

31. Heim R, Cubitt AB, Tsien RY (1995) Improved green fluorescence. *Nature* 373(6516):663–664.

32. Shaner NC, et al. (2004) Improved monomeric red, orange and yellow fluorescent proteins derived from Discosoma sp. red fluorescent protein. *Nat Biotechnol*

22(12):1567–1572.

33. Macdonald PJ, Chen Y, Mueller JD (2012) Chromophore maturation and fluorescence fluctuation spectroscopy of fluorescent proteins in a cell-free expression system. *Anal Biochem* 421(1):291–298.

34. Nagai T, et al. (2002) A variant of yellow fluorescent protein with fast and efficient maturation for cell-biological applications. *Nat Biotechnol* 20(1):87–90.

35. Iizuka R, Yamagishi-Shirasaki M, Funatsu T (2011) Kinetic study of de novo chromophore maturation of fluorescent proteins. *Anal Biochem* 414(2):173–178.

36. Ando R, Mizuno H, Miyawaki A (2004) Regulated fast nucleocytoplasmic shuttling observed by reversible protein highlighting. *Science* 306(5700):1370–1373.

37. Schwanhäusser B, et al. (2011) Global quantification of mammalian gene expression control. *Nature* 473(7347):337–342.

38. Schubert W, et al. (2006) Analyzing proteome topology and function by automated multidimensional fluorescence microscopy. *Nat Biotechnol* 24(10):1270–1278.

39. Zrazhevskiy P, True LD, Gao X (2013) Multicolor multicycle molecular profiling with quantum dots for single-cell analysis. *Nat Protoc* 8(10):1852–1869.

40. Gerdes MJ, Sevinsky CJ, Sood A (2013) Highly multiplexed single-cell analysis of formalin-fixed, paraffin-embedded cancer tissue. *Proc Natl Acad Sci USA* 110(29): 11982–11987.

41. Jungmann R, et al. (2014) Multiplexed 3D cellular super-resolution imaging with DNA-PAINT and Exchange-PAINT. *Nat Meth* 11(3):313–318.

42. Sander JD, Joung JK (2014) CRISPR-Cas systems for editing, regulating and targeting genomes. *Nat Biotechnol* 32(4):347–355.

43. Piston DW, Kremers G-J (2007) Fluorescent protein FRET: the good, the bad and the ugly. *Trends Biochem Sci* 32(9):407–414.

44. Xu J, et al. (2013) Labeling Cytosolic Targets in Live Cells with Blinking Probes. *J Phys Chem Lett* 4(13):2138–2146.

45. Uno S-N, et al. (2014) A spontaneously blinking fluorophore based on intramolecular spirocyclization for live-cell super-resolution imaging. *Nat Chem* 6(8):681-689.

46. Kiuchi T, Higuchi M, Takamura A, Maruoka M, Watanabe N (2015) Multitarget super-resolution microscopy with high-density labeling by exchangeable probes. *Nat Meth* 12(8):743–746.

47. Dertinger T, Colyer R, Iyer G, Weiss S, Enderlein J (2009) Fast, background-free, 3D super-resolution optical fluctuation imaging (SOFI). *Proc Natl Acad Sci USA* 106(52):22287–22292.

48. Blanchard-Desce M, et al. (1997) Large Quadratic Hyperpolarizabilities with Donor-

Acceptor Polyenes Exhibiting Optimum Bond Length Alternation: Correlation Between Structure and Hyperpolarizability. *Chem Eur J* 7:1091–1104.

49. Calamai M, et al. (2009) Gephyrin Oligomerization Controls GlyR Mobility and Synaptic Clustering. *J Neurosci* 29(24):7639–7648.

50. Westerfield M (1994) *The zebrafish book: a guide for the laboratory use of zebrafish Danio (Brachydanio rerio)*.

Table 1. Physico-chemical properties of the fluorogens and their complex with Y-FAST. λ_{abs} wavelength of maximal absorption; λ_{em} wavelength of maximal emission; ε molar absorption coefficient at λ_{abs}; ϕ fluorescence quantum yield; K_D dissociation constant; k_{ON} on-rate kinetic constant; k_{OFF} off-rate kinetic constant. Thermodynamic and kinetic constants are given ± the standard error of the fits (n = 3). Temperature 25°C. [#] The pK_A of HBR is 8.4 ± 0.1. [†] The pK_A of HMBR is 8.7 ± 0.1. [*] Kinetic constants at 25°C were extrapolated from the kinetic parameters shown in **SI Appendix Table S2**. [§] Kinetic constants determined experimentally at 20°C.

	λ_{abs} nm	λ_{em} nm	ε $M^{-1}cm^{-1}$	ϕ %	K_D µM	$10^{-7} \times k_{ON}$ $M^{-1}s^{-1}$	k_{OFF} s^{-1}
HBR (pH 6.8)[#]	397	470	33,000	0.02			
HBR (pH 10.1)[#]	449	545	34,500	0.3			
Y-FAST:HBR (pH 7.4)	467	527	44,000	9	0.62 ± 0.05	3[*] (2.9 ± 0.4[§])	17[*] (8.5 ± 1.2[§])
HMBR (pH 5.8)[†]	401	480	29,500	0.04			
HMBR (pH 10.5)[†]	461	561	33,500	0.2			
Y-FAST:HMBR (pH 7.4)	481	540	45,000	33	0.13 ± 0.01	6.3 ± 0.9	6.3 ± 0.7

FIGURE LEGENDS

Fig. 1. Y-FAST enables specific labeling of fusion proteins in living cells. (a) Y-FAST binds the fluorogenic HBR and HMBR and activates their fluorescence (POI: protein of interest). Binding induces two spectroscopic changes: an increase of the fluorescence quantum yield and an absorption red shift (due to ionization). (**b**) Confocal micrographs of live HeLa cells expressing various Y-FAST fusions labeled with 5 µM HMBR (Ex/Em 488/493-797 nm). Cytoplasm: Y-FAST; Nucleus: H2B-Y-FAST; Cell membrane: Lyn11-Y-FAST; Mitochondria: Mito-FAST (Mito = Mitochondrial targeting sequence from subunit VIII of human cytochrome c oxidase); Golgi: Golgi-Y-FAST (Golgi = N-terminal 81 amino acids of the human beta 1,4-galactosyltransferase); Microtubules: Ensconsin-Y-FAST. **(c)** Epifluorescence micrographs of a dendritic segment of a spinal cord neuron co-transfected with mCerulean-Gephyrin that accumulates at inhibitory synapses (Ex/Em 427/472±15 nm; left panel) and a Y-FAST-tagged Gephyrin construct (Ex/Em 504/542±14 nm; center). After 10 s of incubation with 10 µM HMBR, the fluorescence of Y-FAST was detected in the yellow emission range (Ex/Em 504/542±14 nm; right panel). Scale bars 10 µm.

Fig. 2. Specific labeling of fusion proteins in vivo. Spinning-disk confocal micrographs of live zebrafish embryos co-expressing mCherry/Y-FAST or mCherry/PYP labeled with 5 μM HMBR at 24 hours post-fertilization (HMBR channel: Ex/Em 491/525-539 nm, mCherry channel: Ex/Em 561/605-664 nm; scale bars 200 μm). Side-by-side images were recorded using the same settings.

Fig. 3. On/off fluorescence switching by iterative labeling/unlabeling. (a,b) HeLa cells expressing mCherry-Y-FAST were grown in a microfluidic channel and repeatedly incubated with HMBR-containing culture medium for 20 s and HMBR-free culture medium for 40 s. A multifunctional fluidic controller enabled several cycles of labeling/unlabeling. HMBR concentration was 5 μM. **(a)** Confocal time-lapse showing two cycles of labeling/unlabeling (Ex/Em 488/493-575 nm). **Movie S2** shows ten cycles of labeling/unlabeling. **(b)** Temporal evolution of the cell fluorescence upon addition (+) and removal (–) of HMBR. **(c)** Confocal time-lapse showing the labeling kinetics in a zebrafish embryo expressing Y-FAST and mCherry (HMBR channel: Ex/Em 491/525-539 nm, mCherry channel: Ex/Em 561/605-664 nm). HMBR concentration was 10 μM. See also **Movie S3**. **(d)** A zebrafish embryo expressing Y-FAST and mCherry was imaged before addition of HMBR (–HMBR), 20 min after incubation with 10 μM HMBR (+HMBR), after two washings of 20 min (washing 1 and 2) and after re-incubation with 10 μM HMBR (+HMBR). **(e)** Confocal micrographs of live HeLa cells expressing Dronpa-NLS (nucleus) and lyn11-Y-FAST (membrane) showing sequential imaging of nuclear Dronpa and membrane-anchored Y-FAST through sequential on/off labeling of Y-FAST intercalated with on/off photoswitching of Dronpa (Ex/Em 488/493-797 nm). HMBR concentration was 5 μM. Scale bars 10 μm.

Figure 1

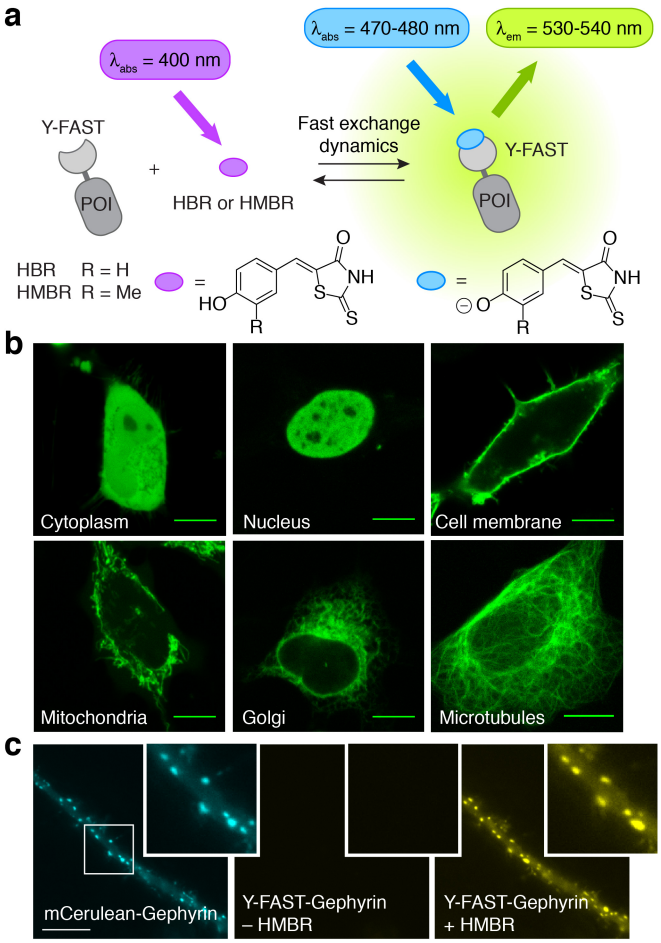
a
λabs = 400 nm
λabs = 470-480 nm
λem = 530-540 nm
Y-FAST
POI
+
HBR or HMBR
Fast exchange dynamics
Y-FAST
POI
HBR R = H
HMBR R = Me
HO
R
NH
S
O
b
Cytoplasm
Nucleus
Cell membrane
Mitochondria
Golgi
Microtubules
c
mCerulean-Gephyrin
Y-FAST-Gephyrin – HMBR
Y-FAST-Gephyrin + HMBR

Figure 2

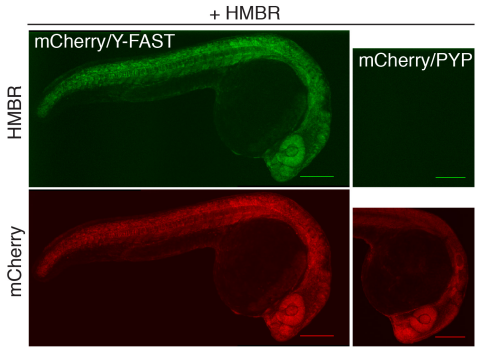

Figure 3

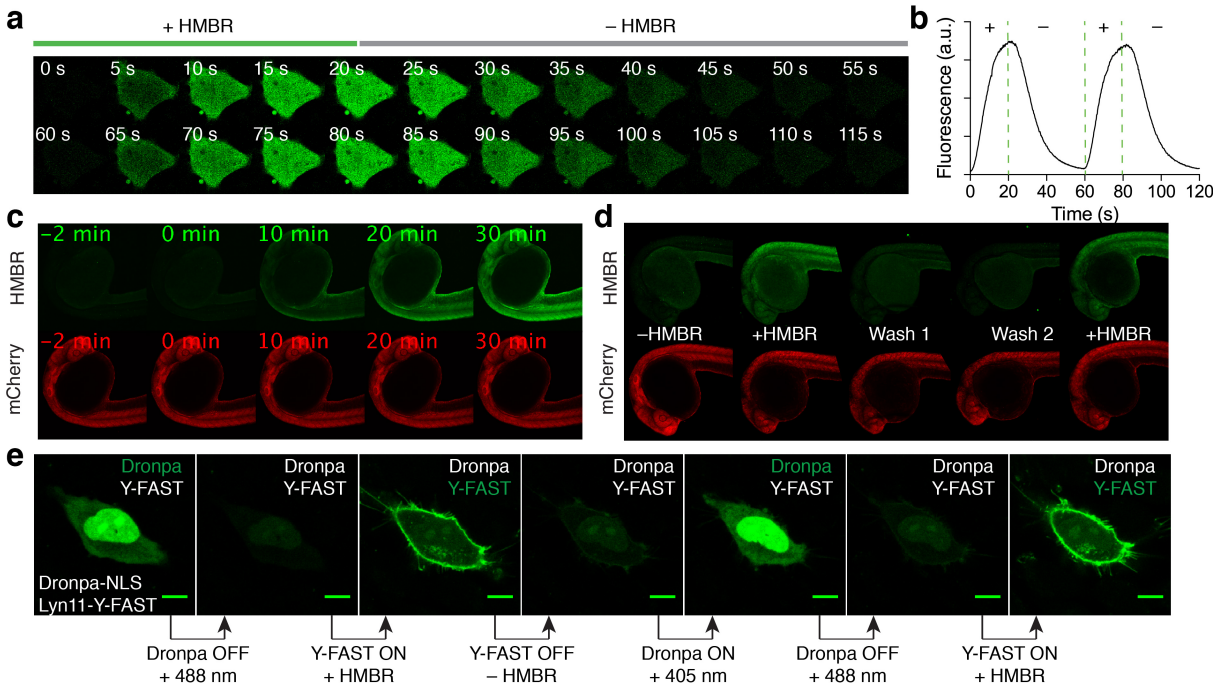
a
+ HMBR
– HMBR
0 s
5 s
10 s
15 s
20 s
25 s
30 s
35 s
40 s
45 s
50 s
55 s
60 s
65 s
70 s
75 s
80 s
85 s
90 s
95 s
100 s
105 s
110 s
115 s
b
Fluorescence (a.u.)
Time (s)
0
20
40
60
80
100
120
c
HMBR
mCherry
–2 min
0 min
10 min
20 min
30 min
d
HMBR
mCherry
–HMBR
+HMBR
Wash 1
Wash 2
+HMBR
e
Dronpa
Y-FAST
Dronpa-NLS
Lyn11-Y-FAST
Dronpa OFF
+ 488 nm
Y-FAST ON
+ HMBR
Y-FAST OFF
– HMBR
Dronpa ON
+ 405 nm
Dronpa OFF
+ 488 nm
Y-FAST ON
+ HMBR

SI Appendix

A small fluorescence-activating and absorption-shifting tag for tunable protein imaging in vivo

Marie-Aude Plamont[a,b,c], Emmanuelle Billon-Denis[a,b,c], Sylvie Maurin[a,b,c], Carole Gauron[d], Frederico M. Pimenta[a,b,c], Christian G. Specht[e], Jian Shi[a,b,c], Jérôme Quérard[a,b,c], Buyan Pan[a,b,c], Julien Rossignol[a,b,c], Nelly Morellet[f], Michel Volovitch[d,e], Ewen Lescop[f], Yong Chen[a,b,c], Antoine Triller[e], Sophie Vriz[d,g], Thomas Le Saux[a,b,c], Ludovic Jullien[a,b,c,1] and Arnaud Gautier[a,b,c,1]

[a] École Normale Supérieure – PSL Research University, Department of Chemistry, 24 rue Lhomond, F-75005 Paris, France.

[b] Sorbonne Universités, UPMC Univ Paris 06, UMR 8640 PASTEUR, F-75005 Paris, France.

[c] CNRS, UMR 8640 PASTEUR, F-75005 Paris, France.

[d] Centre for Interdisciplinary Research in Biology (CIRB) CNRS UMR 7241 / INSERM U1050 / Labex MemoLife, PSL Research University / Collège de France, Paris, France.

[e] École Normale Supérieure, Institute of Biology at the Ecole Normale Supérieure (IBENS), CNRS UMR 8197, INSERM U1024, PSL Research University, 46 rue d'Ulm, Paris 75005, France.

[f] Institut de Chimie des Substances Naturelles, CNRS UPR 2301, Université Paris-Saclay, 1 avenue de la Terrasse, 91198 Gif-sur-Yvette, France.

[g] Université Paris Diderot Sorbonne Paris Cité, Paris, France.

[1] To whom correspondence should be addressed. Email: arnaud.gautier@ens.fr and ludovic.jullien@ens.fr

Contents

SI Figures

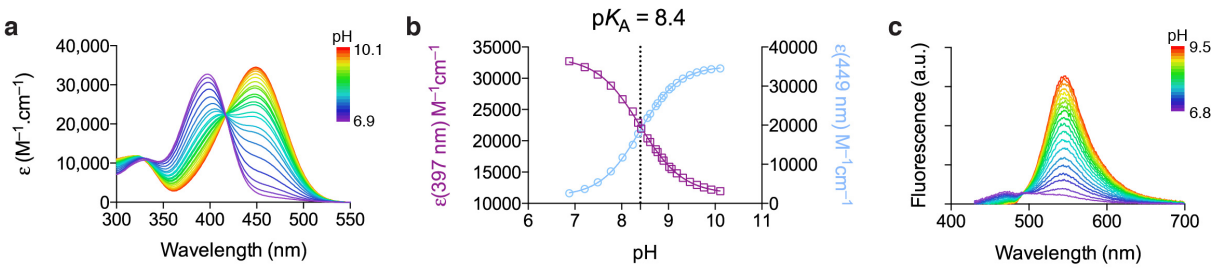

Fig. S1. Spectral properties of HBR in solution in function of pH. (a) Absorption spectra. **(b)** Evolution of the absorption at 397 nm and at 449 nm as a function of pH. **(c)** Fluorescence emission spectra. The spectra were recorded in 0.04 M Britton–Robinson buffer (1) (0.1 M ionic strength) at 25°C.

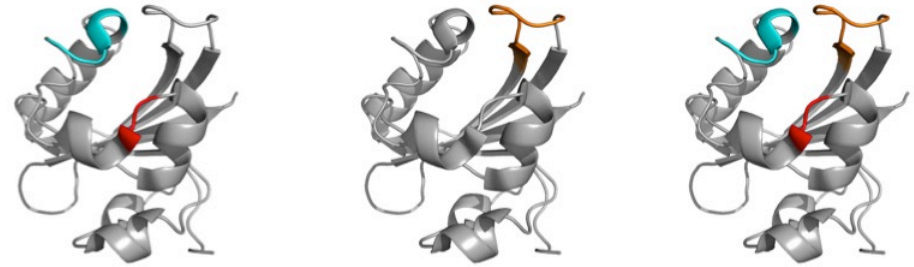

Fig. S2. Libraries of PYP variants. Are indicated the loops within PYP-C69G that were randomized by saturation mutagenesis and the sizes of the final yeast library. The drawings were done using the structure of *Halorhodospira halophila* holo-PYP (PDB: 1NWZ) and the software Pymol.

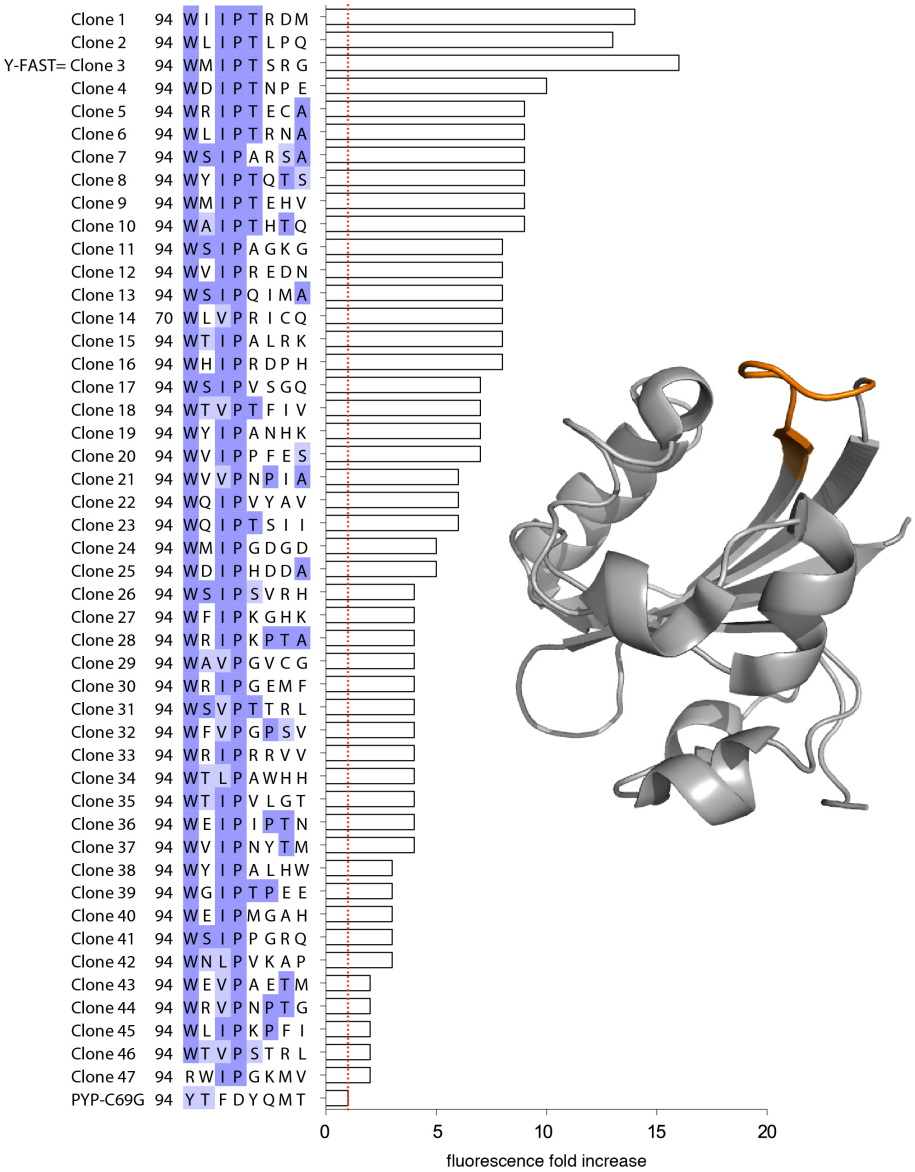

Fig. S3. Sequences of the loop 94-101 (in orange on the structure) found within the clones selected by yeast display. The histogram shows, for each clone, the fluorescence fold increase in presence of 20 µM HBR determined by flow cytometry.

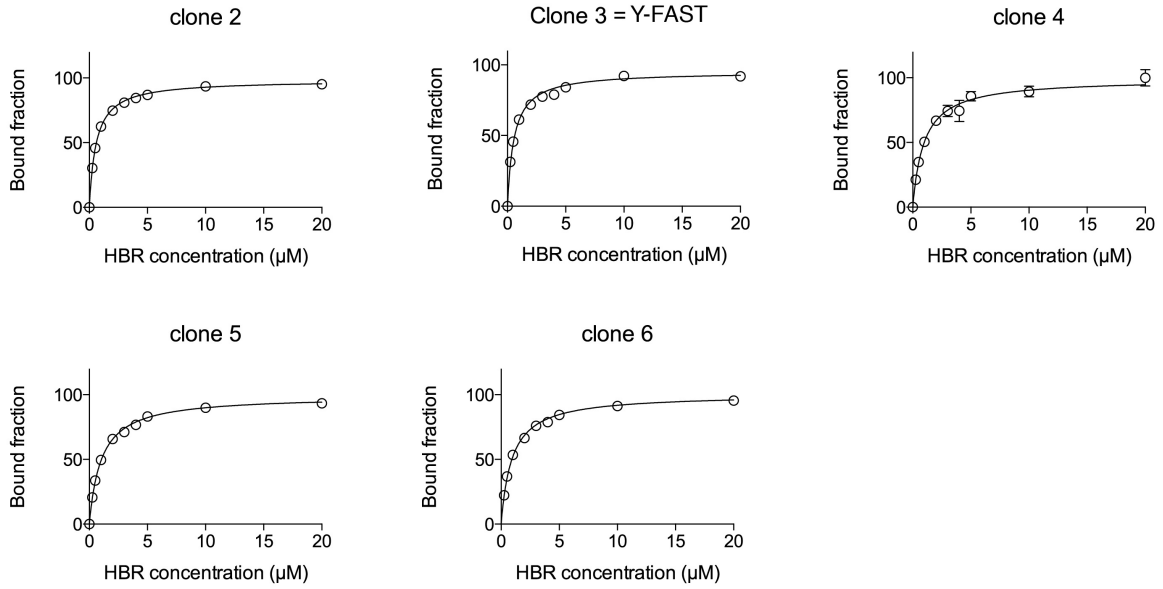

Fig. S4. Affinity of the clones 2-6 for HBR. The graphs show the bound fraction at equilibrium for various HBR concentrations. The protein concentration was 0.1 μM. The titration experiments were performed at 25°C in pH 7.4 PBS (50 mM sodium phosphate, 150 mM NaCl). Data represent mean ± sem (n = 3 or 4). Least squares fit (line) gave the dissociation constants K_D presented in **Table 1** and **Table S1**.

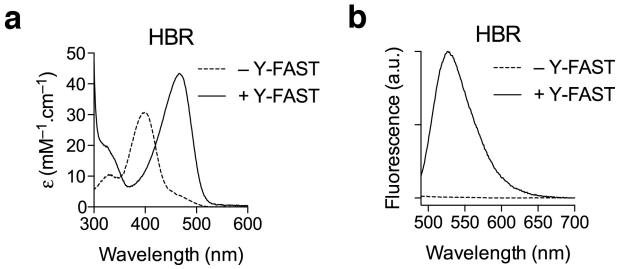

Fig. S5. Absorption **(a)** and emission **(b)** spectra of HBR ± Y-FAST. HBR and Y-FAST concentrations were 2 μM and 40 μM, respectively, in pH 7.4 PBS (50 mM sodium phosphate, 150 mM NaCl). Spectra were recorded at 25°C.

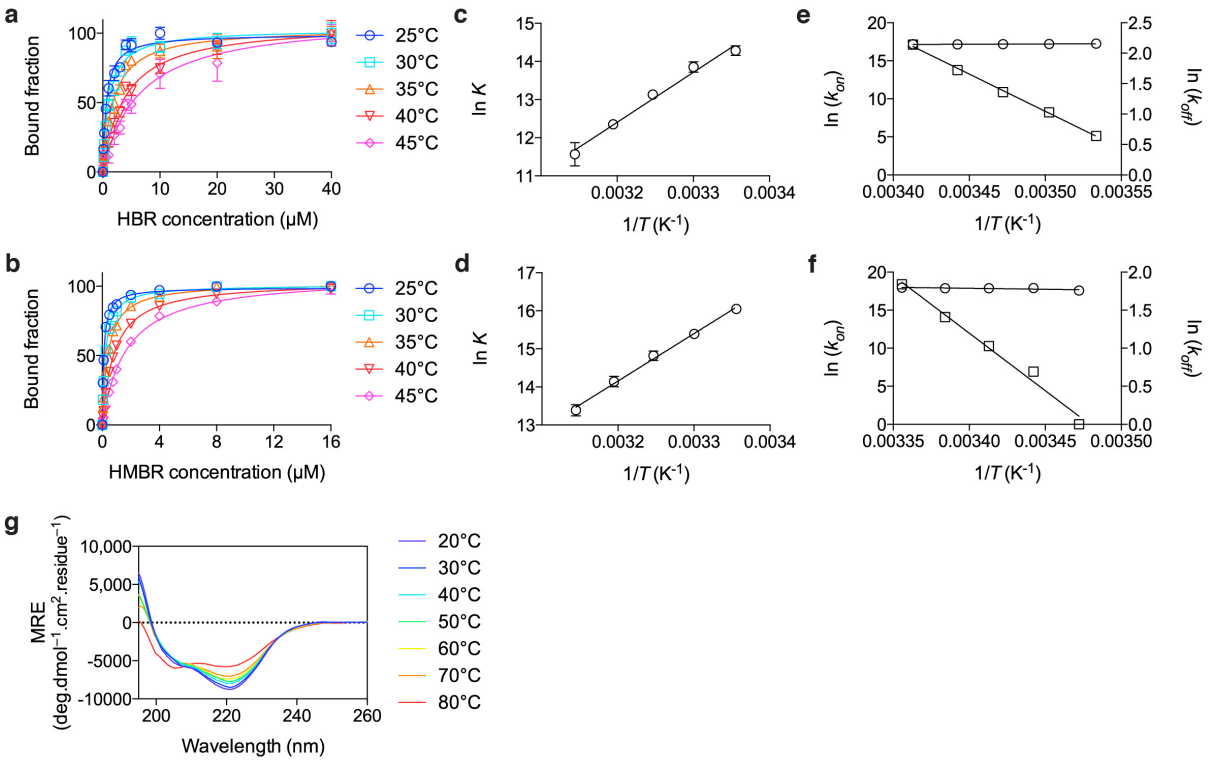

Fig. S6. Thermokinetic analysis of the binding of HBR and HMBR with Y-FAST. (a,b) Evolution of the bound fraction at equilibrium as a function of **(a)** HBR and **(b)** HMBR concentrations at various temperatures. Y-FAST concentration was 100 nM **(a)** or 50 nM **(b)**. The titration experiments were performed in pH 7.4 PBS (50 mM sodium phosphate, 150 mM NaCl). Data represent mean ± sem (n = 4). Least squares fit (line) gave the dissociation constant $K_D = 1/K$. **(c,d)** Dependence of ln$K$ on $1/T$ for **(c)** HBR and **(d)** HMBR (values represent the mean ± SD of 3 independent K_D determinations as shown in **(a)** and **(b)**). The enthalpy ΔH^0 and entropy ΔS^0 of binding were extracted using the expression: $\ln K = -\Delta H^0/RT + \Delta S^0/R$ (see **Table S2**). **(e,f)** Dependence of ln(k_{on}) (circles) and ln(k_{off}) (squares) on $1/T$ for **(e)** HBR and **(f)** HMBR (see **Table S3** for the values). The values of A_{on} and A_{off} and $E_{a,on}$ and $E_{a,off}$ denoting the frequency factors, and the activation energies of the forward and backward kinetic constants, respectively, were determined using: $k_{on} = A_{on} \exp(-E_{a,on}/RT)$ and $k_{off} = A_{off} \exp(-E_{a,off}/RT)$. **(g)** Circular dichroism spectra of Y-FAST at various temperatures. Buffer: pH 7.4 PBS (50 mM sodium phosphate, 150 mM NaCl). MRE: mean residue ellipticity.

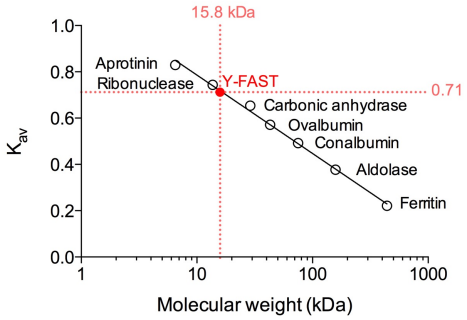

Fig. S7. Y-FAST appears as a monomer in size-exclusion chromatography. The oligomeric state of Y-FAST was analyzed by size-exclusion chromatography at 25°C by injecting a solution of Y-FAST at 1.25 mM in pH 7.4 PBS (50 mM sodium phosphate, 150 mM NaCl). The partition coefficient (K_{av}) is plotted against molecular weight (kDa) for known proteins (black circles). Y-FAST eluted with a partition coefficient of 0.71 (red circle) giving an apparent molecular weight of 15.8 kDa in good agreement with its theoretical size of 14 kDa.

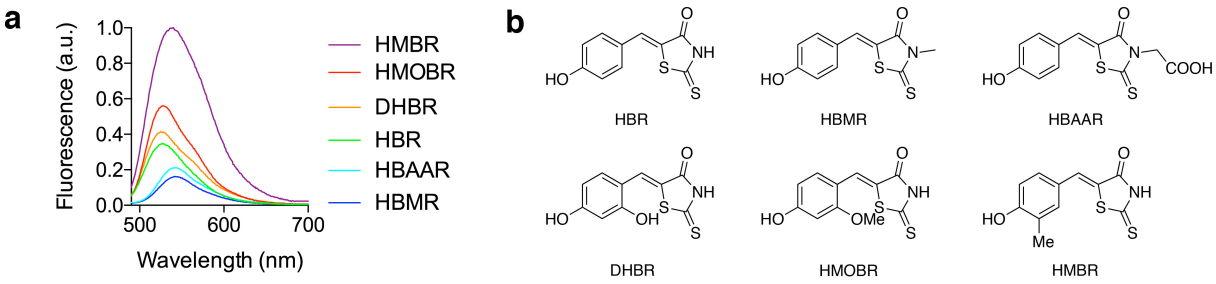

Fig. S8. Fluorescence spectra **(a)** of various HBR analogs **(b)** in presence of Y-FAST. HBR analogs (2 µM) were incubated with Y-FAST (40 µM) in pH 7.4 PBS (50 mM sodium phosphate, 150 mM NaCl). Spectra were recorded at 25°C (Ex 470 nm) with the same settings for direct comparison.

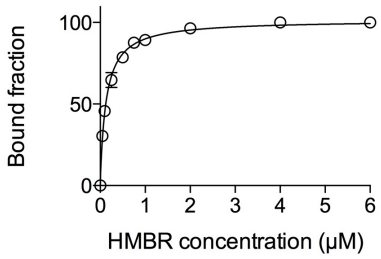

Fig. S9. Affinity of Y-FAST for HMBR. The graph shows the bound fraction at equilibrium for various HMBR concentrations. Y-FAST concentration was 50 nM. The titration experiments were performed at 25°C in pH 7.4 PBS (50 mM sodium phosphate, 150 mM NaCl). Data represent mean ± sem (n = 4). Least squares fit (line) gave the dissociation constant K_D reported in **Table 1**.

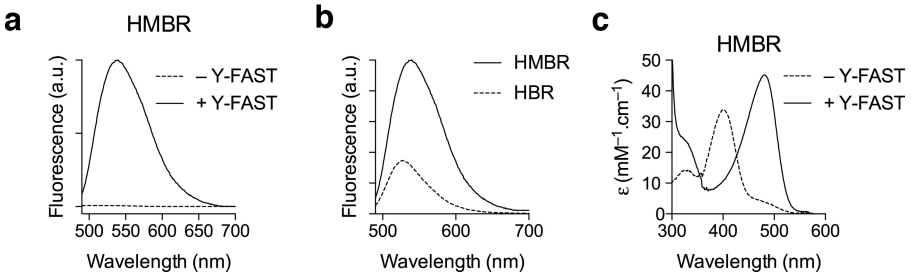

Fig. S10. (a) Fluorescence emission spectra of HMBR ± Y-FAST. **(b)** Relative fluorescence emission of HBR and HMBR bound to Y-FAST. **(c)** Absorption spectra of HMBR ± Y-FAST. HBR, HMBR and Y-FAST concentrations were 2 µM, 2 µM and 40 µM, respectively, in pH 7.4 PBS (50 mM sodium phosphate, 150 mM NaCl). Spectra were recorded at 25°C.

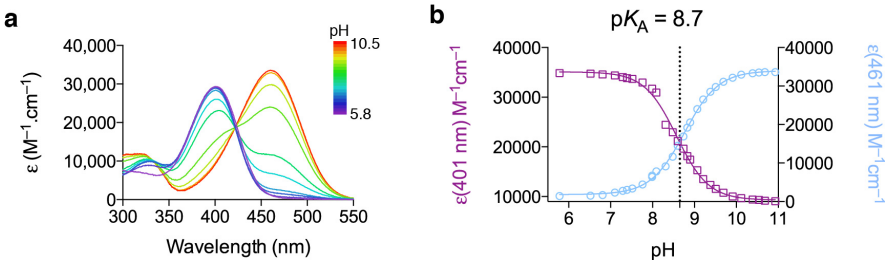

Fig. S11. Spectral properties of HMBR in solution in function of pH. (a) Absorption spectra at various pH. **(b)** Evolution of the absorption at 401 nm and at 461 nm as a function of pH. The spectra were recorded in 0.05 M Britton–Robinson buffer (1) (0.28 M ionic strength) at 25°C.

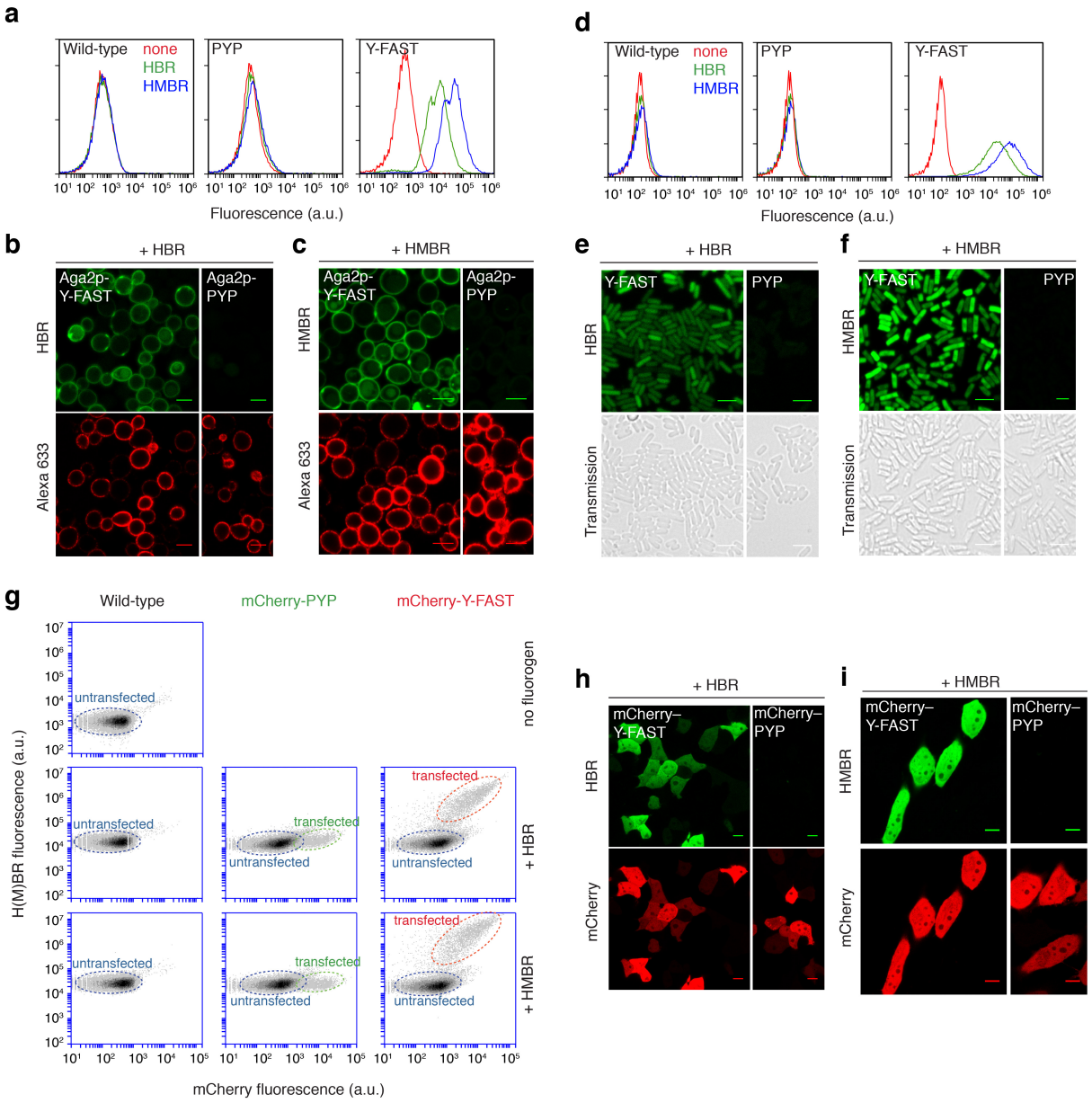

Fig. S12. Labeling of Y-FAST with HBR and HMBR in yeast, bacteria and mammalian cells. (a) *S. cerevisiae* wild-type cells or cells expressing Aga2p fused either to Y-FAST or to PYP were incubated with 20 µM HBR (green) or 20 µM HMBR (blue) or without dye (red), and analyzed by flow cytometry. See **Table S5** for the quantification**. (b,c)** Confocal micrographs of *S. cerevisiae* cells expressing Aga2p fused either to Y-FAST or to PYP-C69G and incubated with 20 µM HBR **(b)** or 5 µM HMBR **(c)**; the Aga2p fusion protein was immunolabeled with an Alexa633-conjugated antibody (H(M)BR channel: Ex/Em 488/493-600 nm; Alexa633 channel: Ex/Em 633/638-797 nm, scale bars 5 µm). **(d)** *E. coli* wild-type cells or cells expressing Y-FAST or PYP were incubated with 20 µM HBR (green) or 20 µM HMBR (blue) or without dye (red), and analyzed by flow cytometry. See **Table S5** for the quantification. **(e,f)** Confocal micrographs of *E. coli* cells expressing either His-tagged Y-FAST or His-tagged PYP-C69G incubated with 20 µM HBR **(e)** or 5 µM HMBR **(f)** (Ex/Em 488/493-797 nm, scale bars 3 µm). **(g)** HeLa wild-type cells or cells expressing mCherry-Y-FAST or mCherry-PYP were incubated with 20 µM HBR (green) or 20 µM HMBR (blue) or

without dye (red), and analyzed by flow cytometry. See **Table S5** for the quantification. **(h,i)** Confocal micrographs of mammalian cells expressing mCherry-Y-FAST or mCherry-PYP labeled with 20 μM HBR **(h)** or 5 μM HMBR **(i)** (H(M)BR: Ex/Em 488/493-575 nm; mCherry: Ex/Em 543/578-797 nm; scale bars 10 μm).

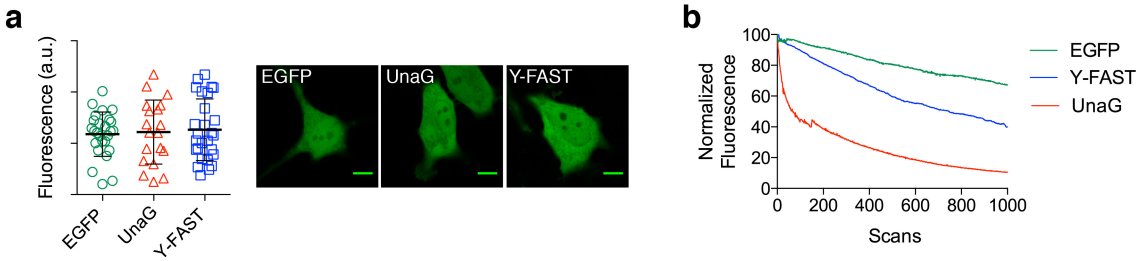

Fig. S13. Comparison of Y-FAST with EGFP and UnaG. (a) Fluorescence of HeLa cells (n = 15-30) expressing EGFP, UnaG and Y-FAST (labeled with 5 µM HMBR) and imaged using the same settings for direct comparison of the fluorescence intensities. The images on the right hand side are confocal micrographs of representative cells (Ex/Em 488/493-797 nm; scale bars 10 µm). **(b)** Photoresistance in cells. Fluorescence levels of HeLa cells expressing EGFP, Y-FAST (labeled with 5 µM HMBR) and UnaG upon long-term observation with high power 488 nm laser excitation (light power 90 kW.cm^{-2}, pixel dwell 1.58 µs). Plots show the fluorescence intensity as a function of the number of confocal microscope scans.

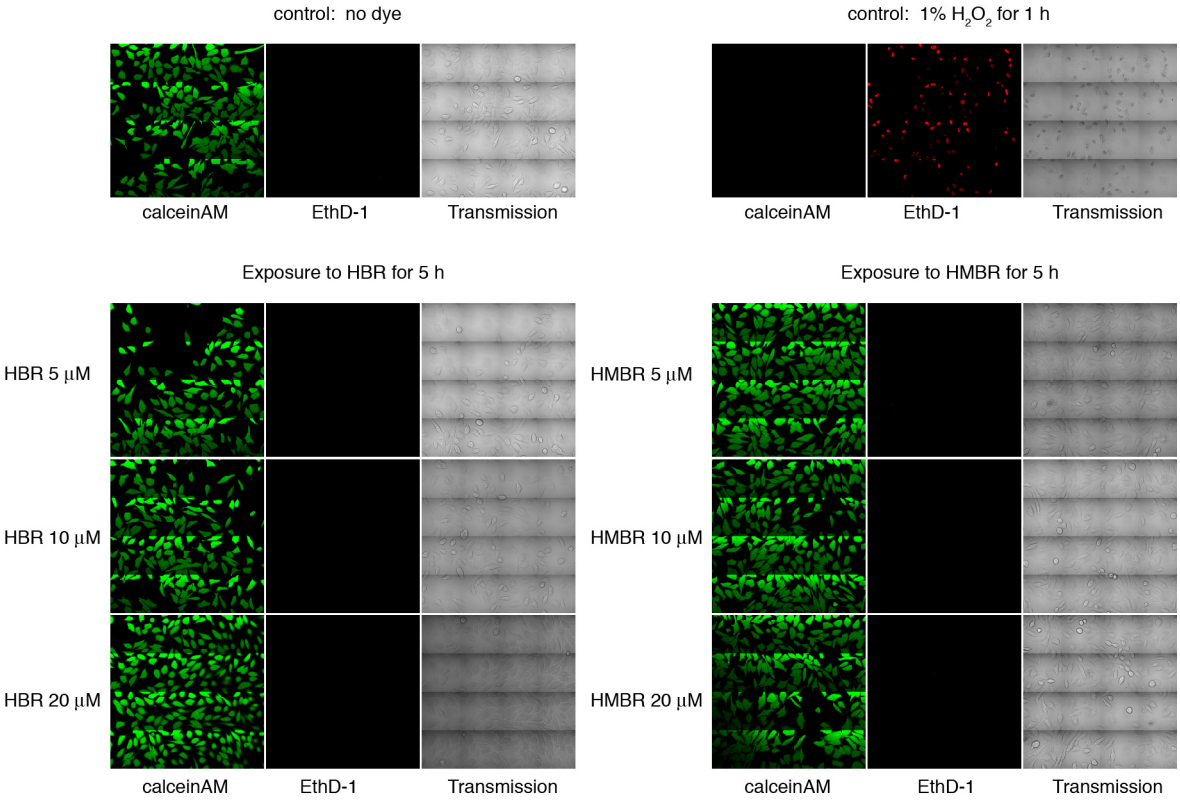

Fig. S14. Viability assay of HeLa cells incubated for 5 h with solutions of HBR and HMBR at 5, 10 and 20 μM. Cell viability was tested by using calceinAM and EthD1 (LIVE/DEAD® viability/cytotoxicity assay kit). CalceinAM is a cell-permeant profluorophore cleaved by intracellular esterases releasing the green fluorescent polyanionic calcein in live cells. EthD1 (Ethidium homodimer 1) is a non cell-permeant nucleic acid red fluorescent stain that enters only cells with damaged membranes and undergoes a fluorescence enhancement upon binding to nucleic acids, thereby producing a bright red fluorescence in dead cells. Control experiments with HeLa cells non-incubated with dye (top left, live control) or incubated for 1 h with 1% hydrogen peroxyde (top right, dead control) are shown. Cell fluorescence was evaluated by confocal microscopy. The experiment shows that HBR and HMBR are non-toxic for HeLa cells at the concentrations used for imaging.

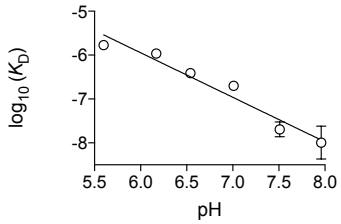

Fig. S15. Influence of pH on Y-FAST properties. (a) Evolution of log K_D in function of pH, where K_D is the dissociation constant of Y-FAST:HMBR. Titration experiments were performed in an adapted Britton-Robinson universal buffer (using 50 mM sodium acetate, N-(1,1-Dimethyl-2-hydroxyethyl)-3-amino-2-hydroxypropanesulfonic acid (AMPSO) and sodium phosphate) at 25°C.

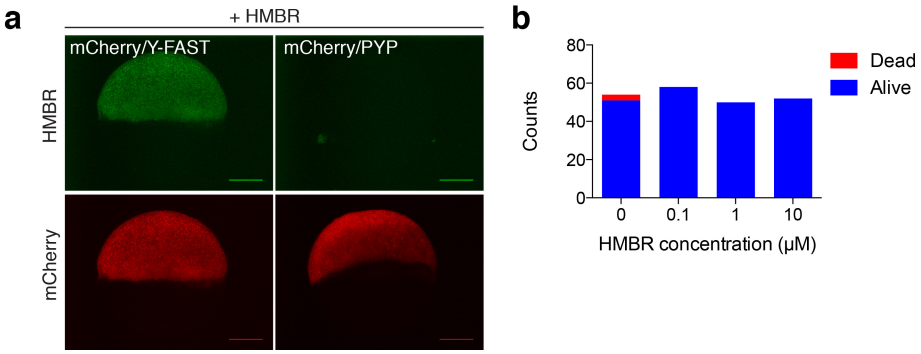

Fig. S16. Labeling of fusion proteins in zebrafish. (a) Spinning-disk confocal micrographs of live zebrafish embryos co-expressing mCherry/Y-FAST or mCherry/PYP labeled with 5 µM HMBR during gastrulation (HMBR channel: Ex/Em 491/525-539 nm, mCherry channel: Ex/Em 561/605-664 nm; scale bars 200 µm). Side-by-side images were recorded using the same settings. **(b)** Viability of zebrafish embryos incubated with HMBR during development from 50 % epiboly to 24 hpf (19 hours of incubation). The plot shows for various HMBR concentrations the number of embryos that were alive with no morphological defect (blue) or dead (red) at 24 hpf.

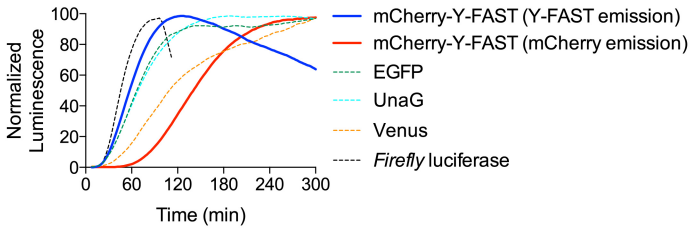

Fig. S17. Monitoring of protein synthesis in near real-time. A gene encoding Y-FAST fused to mCherry (mCherry-Y-FAST) was expressed in vitro in the cell-free PURE system in presence of 5 µM HMBR at 37°C. The solid blue line shows the temporal evolution of Y-FAST emission while the solid red line shows the temporal evolution of mCherry emission. Note that the drop of Y-FAST emission over time reflects mainly the energy transfer to mature mCherry (see also discussion). The plot also shows the temporal luminescence evolution during in vitro synthesis of EGFP (green dashed line), UnaG in presence of 5 µM bilirubin (cyan dashed line), Venus (orange dashed line) and *Firefly* luciferase in presence of luciferin (black dashed line). In all the experiments, the genes were under the control of the same T7 promoter. Data represent the mean of three replicates.

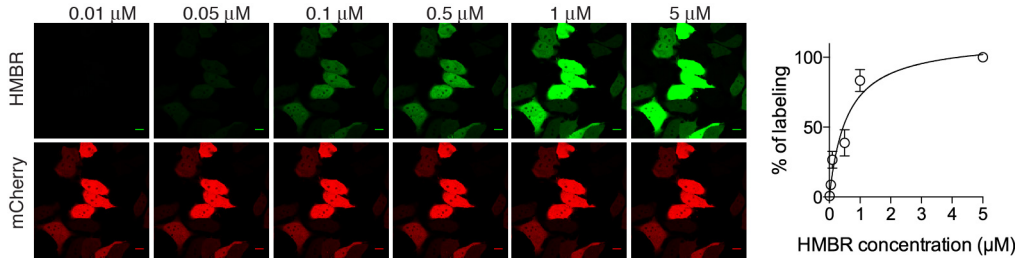

Fig. S18. Y-FAST enables the control of the density of fluorescent labeling independently of the expression level. Confocal micrographs of live HeLa cells expressing mCherry fused to Y-FAST incubated with various concentrations of HMBR (HMBR channel: Ex/Em 488/493-575 nm, mCherry channel: Ex/Em 543/578-797 nm; scale bars 10 µm). Plot shows the percentage of labeling as a function of the concentration. Data represents mean ± SD (n = 15).

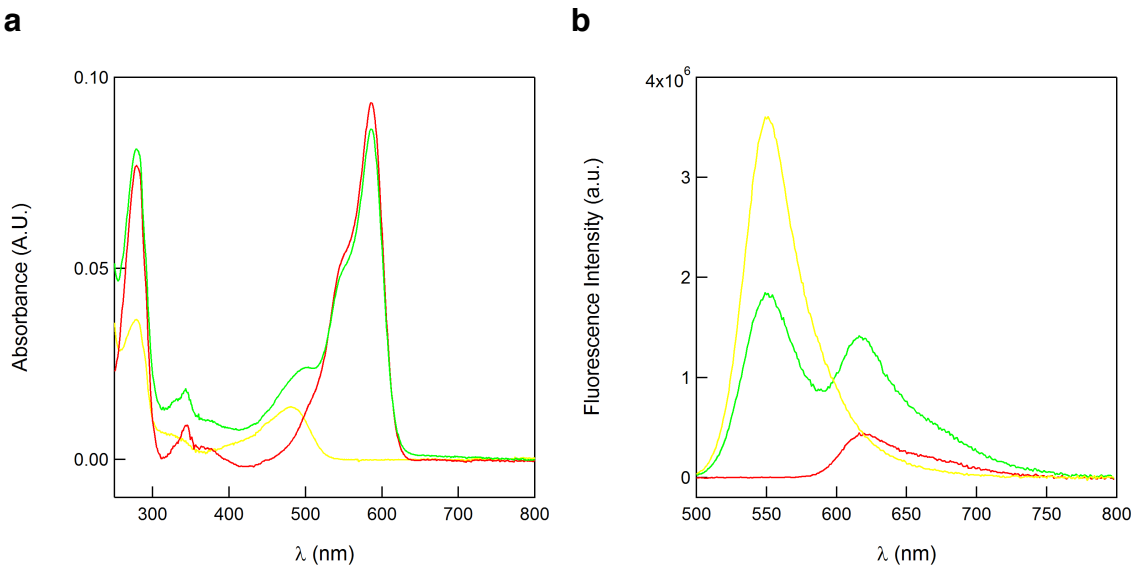

Fig. S19. FRET efficiency determination. Absorption (**a**) and emission (λ_{exc} = 470 nm; (**b**) spectra of 1.5 µM Y-FAST in the presence of 250 nM HMBR (yellow solid line) and of 1.5 µM Y-FAST-mCherry in the absence (red solid line) or in the presence (green solid line) of 250 nM HMBR. Buffer: pH 7.4 PBS (50 mM sodium phosphate, 150 mM NaCl). Temperature: 25°C.

SI Tables

Table S1. Thermodynamic and photophysical properties of selected clones. K_D dissociation constant of the complex with HBR (± standard error of the fits, n = 3; see **Fig. S4** for the experimental data); λ_{abs} wavelength of maximal absorption; λ_{em} wavelength of maximal emission; ε molar absorption coefficient at λ_{abs}; ϕ fluorescence quantum yield. Buffer: pH 7.4 PBS (50 mM sodium phosphate, 150 mM NaCl). Temperature: 25°C.

Protein	Res. 94-101	K_D (μM)	λ_{abs} (nm)	λ_{em} (nm)	ε ($M^{-1}cm^{-1}$)	ϕ (%)
#2	WLIPTLPQ	0.59 ± 0.02	466	530	46,000	6
#3/Y-FAST	WMIPTSRG	0.62 ± 0.05	467	527	44,000	9
#4	WDIPTNPE	0.97 ± 0.08	468	531	41,000	6
#5	WRIPTECA	1.02 ± 0.03	468	532	47,000	6
#6	WLIPTRNA	0.93 ± 0.03	467	529	43,000	7
PYP-C69G	YTFDYQMT					

Table S2. Thermokinetic parameters associated to the binding of HBR and HMBR to Y-FAST. ΔH^0 and ΔS^0 denote the enthalpy and entropy of binding. A_{on} and A_{off}, and $E_{a,on}$ and $E_{a,off}$ respectively denote the frequency factors, and the activation energies of the on-rate and off-rate kinetic constants defined by $k_{on} = A_{on} \exp(-E_{a,on}/RT)$ and $k_{off} = A_{off} \exp(-E_{a,off}/RT)$. Values are given with the standard error of the fits. See **Fig. S6** for the experimental data.

Fluorogen	ΔH^0 ($kJ.mol^{-1}$)	ΔS^0 ($J.K^{-1}.mol^{-1}$)	$\ln(A_{on})$	$\ln(A_{off})$	$E_{a,on}$ ($kJ.mol^{-1}$)	$E_{a,off}$ ($kJ.mol^{-1}$)
HBR	–109 ± 6	–245 ± 18	16 ± 2	45 ± 1	–3 ± 3	103 ± 6
HMBR	–104 ± 3	–214 ± 10	26 ± 3	53 ± 4	21 ± 10	124 ± 12

Table S3. On-rate (k_{on}) and off-rate (k_{off}) kinetic constants for HBR and HMBR at various temperatures. Values are given with the standard error of the fits (n = 3).

Temperature (°C)	$10^{-7} \times k_{on}$(HBR) ($M^{-1}s^{-1}$)	k_{off}(HBR) (s^{-1})	$10^{-7} \times k_{on}$(HMBR) ($M^{-1}s^{-1}$)	k_{off}(HMBR) (s^{-1})
10	3.1 ± 0.4	1.9 ± 0.3	-	-
12.5	3.0 ± 0.4	2.8 ± 0.5	-	-
15	2.9 ± 0.4	3.9 ± 0.6	4.3 ± 0.5	1.0 ± 0.2
17.5	2.8 ± 0.4	5.6 ± 0.8	6.0 ± 0.9	2.0 ± 0.3
20	2.9 ± 0.4	8.5 ± 1.2	5.8 ± 0.8	2.8 ± 0.4
22.5	-	-	5.9 ± 0.8	4.1 ± 0.5
25	-	-	6.3 ± 0.9	6.3 ± 0.7

Table S4. Hydrodynamic parameters obtained from ^{15}N NMR relaxation and DOSY experiments compared with the parameters predicted for the monomeric Y-FAST ± HBR. $\tau_{c,exp}$ and $\tau_{c,predicted}$ are respectively the tumbling time determined experimentally by the ^{15}N relaxation NMR experiments and predicted by HydroNMR. *D*, r_H, *N* and MW are respectively the translational diffusion coefficient, the hydrodynamic radius, the number of residues and the molecular weight obtained from the DOSY experiments. The calculated viscosity η is also given.

	T (K)	$\tau_{c,exp}$ (ns)	$\tau_{c,predicted}$ (ns)	*D* ($m^2.s^{-1}$)	r_H (nm)	*N*	MW (Da)	η (Pa·s)
– HBR	278	12.0 ± 0.1	12.7	7.08×10^{-11}	1.89	118	12,980	0.0015488
	293	8.0 ± 0.1	8.05	1.10×10^{-10}	1.95	130	14,300	0.0010350
+ HBR	278	12.1 ± 0.1	12.7	7.24×10^{-11}	1.85	109	11,990	0.0015488
	293	7.4 ± 0.05	8.05	1.14×10^{-10}	1.87	113	12,430	0.0010350

Table S5. Flow cytometry analysis of Y-FAST labeling in *S. cerevisiae*, *E. coli* and HeLa cells. The fluorescence of cells expressing fusions to PYP or Y-FAST and incubated with HBR or HMBR was quantified by flow cytometry (see plots on **Fig. S12**). The table presents the mean fluorescence, the coefficient of variation (CV), and the fluorescence fold-increase relative to wild-type cells incubated with the given fluorogen.

S. cerevisiae

	Wild-type		PYP			Y-FAST		
Fluorogen	Mean Fluo.	CV	Mean Fluo.	CV	Fold increase	Mean Fluo.	CV	Fold increase
–	623	95%	565	112%		692	109%	
HBR	634	253%	710	236%	1.1	13,645	133%	22
HMBR	638	183%	781	153%	1.2	52,143	129%	82

E. coli

	Wild-type		PYP			Y-FAST		
Fluorogen	Mean Fluo.	CV	Mean Fluo.	CV	Fold increase	Mean Fluo.	CV	Fold increase
–	168	60%	173	58%		175	63%	
HBR	187	486%	182	72%	1.0	35,673	148%	191
HMBR	192	112%	180	95%	0.9	105,472	157%	550

HeLa cells

	Wild-type		PYP			Y-FAST		
Fluorogen	Mean Fluo.	CV	Mean Fluo.	CV	Fold increase	Mean Fluo.	CV	Fold increase
–	1,959	45%						
HBR	18,524	36%	20,401	33%	1.1	1,179,473	91%	64
HMBR	27,728	40%	24,430	26%	0.9	3,048,055	84%	110

SI Texts

Text S1: Measurement of the thermokinetic properties of the fluorogen/protein complexes

The model

Considering that the fluorogen and the protein interact to provide a fluorescent complex, we adopted a two-state model to analyze the thermodynamics and the kinetics of the interaction. Denoting the fluorogen, the protein and the complex respectively **A**, **B**, and **AB**, the interaction

$$\mathbf{A} + \mathbf{B} \quad \rightleftarrows \quad \mathbf{AB} \qquad [1]$$

is characterized by the rate constants k_{on} and k_{off} associated to the forward and backward reactions respectively, and the association thermodynamic constant K (= $1/K_D$) equal to the ratio k_{on}/k_{off}.

Calculation of the equilibrium state

A_{tot} and B_{tot} denoting the total concentrations of **A** and **B**, the final concentrations A_{fin}, B_{fin}, and AB_{fin} of the three species **A**, **B**, and **AB** at equilibrium are

$$AB_{fin} = \frac{[K(A_{tot}+B_{tot})+1]-\sqrt{[K(A_{tot}+B_{tot})+1]^2-4K^2A_{tot}B_{tot}}}{2K} \qquad [2]$$

$$A_{fin} = A_{tot} - AB_{fin} \qquad [3]$$

$$B_{fin} = B_{tot} - AB_{fin} \qquad [4]$$

When $A_{tot} \gg B_{tot}$ as in the present series of experiments, the expressions [2-4] become

$$AB_{fin} = \frac{KA_{tot}}{KA_{tot}+1} B_{tot} \qquad [5]$$

$$A_{fin} = A_{tot} \qquad [6]$$

$$B_{fin} = \frac{1}{KA_{tot}+1} B_{tot} \qquad [7]$$

Measurement of the association constant K

The experimental observable is the fluorescence emission. Neglecting the brightness of the empty protein **B**, the fluorescence intensity I_F results from the contributions of the fluorogen **A** and its complex **AB** with respective brightnesses Q_A and Q_{AB} such that:

$$I_F = Q_A A + Q_{AB} AB \quad [8]$$

The thermodynamic constant K was determined by analyzing the dependence of the fluorescence intensity I_F on the total concentration of the fluorogen A_{tot} at constant concentration of the protein B_{tot}. We first extracted the bound fraction equal to AB_{fin}/B_{tot} by (i) correcting $I_F(A_{tot})$ from the free fluorogen contribution ($Q_A A_{tot}$) and (ii) dividing the resulting corrected fluorescence intensity $I_{F,corr}(A_{tot})$ by its upper value $I^{\infty}_{F,corr}$ at large enough A_{tot} concentrations such that $AB_{fin} = B_{tot}$. We subsequently fitted the dependence of the bound fraction on A_{tot} with Eq.[9] derived from Eq.[8] to retrieve K.

$$\frac{AB_{fin}}{B_{tot}} = \frac{I_{F,corr}(A_{tot})}{I^{\infty}_{F,corr}} = \frac{I_F - Q_A A_{tot}}{I^{\infty}_{F,corr}} = \frac{KA_{tot}}{KA_{tot}+1} \quad [9]$$

Dependence on temperature of the association constant K

The association constant K for HBR and HMBR was determined at different temperatures in the 25-45°C range in order to obtained the enthalpy ΔH^0 and the entropy ΔS^0 associated with the reaction [1] (**Fig. S6a-d**). Using circular dichroism, we verified that Y-FAST was stable in the considered temperature range (**Fig. S6g**) in order to ascertain that our two-state model was valid for the subsequent analyses.

We extracted the enthalpy ΔH^0 and the entropy ΔS^0 associated with the reaction [1] from the linear dependence of $\ln K$ on $1/T$ given in Eq.[10], which has been derived by assuming that ΔH^0 and ΔS^0 do not depend on temperature in the considered temperature range

$$\ln K(T) = -\frac{\Delta H^0}{RT} + \frac{\Delta S^0}{R} \quad [10]$$

Fig. S6c,d display the linear dependences observed for HBR and HMBR from which we extracted the values of ΔH^0 and ΔS^0 given in **Table S2**.

Calculation of the temporal evolution of the concentrations

We next extracted the rate constants k_{on} and k_{off} from the temporal evolution of the concentrations A, B, and AB of the three species **A**, **B**, and **AB** using stopped-flow experiments.

Considering that the two feeding syringes respectively contain **A** and **B** such that their respective initial concentrations in the cuvette after fast mixing are A_{tot} and B_{tot}, the instantaneous concentrations of **A**, **B**, and **AB** in the cuvette, A, B, and AB, monotonously evolve towards the equilibrium concentrations A_{fin}, B_{fin}, and AB_{fin} that are given by the expressions [2-4].

The differential equation governing the temporal evolution of the concentrations A, B, and AB is

$$-\frac{dA}{dt} = -\frac{dB}{dt} = \frac{dAB}{dt} = k_{on}A\times B - k_{off}AB \quad [11]$$

Following a development previously reported (2), we obtained

$$AB = AB_{fin}\left\{1 - \frac{\exp\left(-\frac{t}{\tau}\right)}{1+AB_{fin}k_{on}\tau\left[1-\exp\left(-\frac{t}{\tau}\right)\right]}\right\} \quad [12]$$

$$A = A_{tot} - AB \quad [13]$$

$$B = B_{tot} - AB \quad [14]$$

with

$$\tau = \frac{1}{k_{on}(A_{fin}+B_{fin})+k_{off}} \quad [15]$$

Measurement of the rate constants k_{on} and k_{off}

Extraction of the rate constants k_{on} and k_{off} at a given temperature has been performed by analyzing the temporal dependence of the fluorescence intensity in a series of stopped-flow experiments. We first derived Eq.(16) from Eqs.(8,12,13).

$$I_F(t) = Q_A A_{tot} + (Q_{AB} - Q_A)AB_{fin}\left\{1 - \frac{\exp\left(-\frac{t}{\tau}\right)}{1+AB_{fin}k_{on}\tau\left[1-\exp\left(-\frac{t}{\tau}\right)\right]}\right\} \quad [16]$$

Upon noting after preliminary fits and simulations that $AB_{fin}k_{on}\tau \ll 1$, we could further simplify the fitting equation and eventually adopted Eq.(17) to extract the relaxation time τ.

$$I_F(t) = Q_A A_{tot} + (Q_{AB} - Q_A)AB_{fin}\left\{1 - \exp\left(-\frac{t}{\tau}\right)\right\} \quad [17]$$

Above 25°C, the relaxation time τ was below the temporal resolution of our stopped-flow instrument under the relevant conditions of initial concentrations A_{tot} and B_{tot} to perform this series of experiments. Therefore we considered to measure the relaxation time and the rate constants k_{on} and k_{off} at lower temperatures, and to subsequently extrapolate their values at higher temperatures by adopting the Arrhenius expression to account for the temperature-dependence of the rate constants $k_{on}(T)$ and $k_{off}(T)$

$$k_{on}(T) = A_{on}\exp\left(-\frac{E_{a,on}}{RT}\right) \quad [18]$$

$$k_{off}(T) = A_{off}\exp\left(-\frac{E_{a,off}}{RT}\right) \quad [19]$$

where A_{on} and A_{off}, and $E_{a,on}$ and $E_{a,off}$ denote the frequency factors, and the activation energies associated with the forward and backward reaction [1], respectively.

We used two different approaches to extract the rate constants k_{on} and k_{off} from the relaxation time τ:

- We first measured τ at 15°C in a series of experiments in which we used various initial concentrations A_{tot} and B_{tot}. This series of experiments enabled to independently extract k_{on} and k_{off} at 15°C: We found $(2.5 \pm 0.4) \times 10^7$ $M^{-1}s^{-1}$ and 4.1 ± 0.7 s^{-1}, and $(2.0 \pm 0.5) \times 10^7$ $M^{-1}s^{-1}$ and 2.1 ± 0.5 s^{-1} for HBR and HMBR respectively;

- We then measured τ at various temperatures spanning the 10-25°C range in series of experiments in which we used various initial concentrations A_{tot} and B_{tot}. The latter variations being too narrow to independently extract k_{on} and k_{off} as above, we relied on the expression $K = k_{on}/k_{off}$ and on the temperature-dependence of the association constant K to extract the values of k_{on} and k_{off} from the relaxation time τ in the considered temperature range (**Table S3**). In particular, the values of k_{on} and k_{off} extracted at 15°C were in close agreement with the values determined previously. **Fig. S6e,f** display the dependence of $\ln(k_{on})$ and $\ln(k_{off})$ on $1/T$ for HBR and HMBR. They both exhibit the linear dependence expected from Eqs.[18,19]. We correspondingly used Eqs.[18,19] to extract A_{on} and A_{off}, and $E_{a,on}$ and $E_{a,off}$ given in **Table S2**.

Text S2: Analysis of the oligomeric state of Y-FAST by NMR spectroscopy

We used NMR spectroscopy to assess the oligomeric state of Y-FAST under various conditions in solution. The global tumbling correlation time τ_c and the translational diffusion coefficient *D* are hydrodynamic properties that are highly sensitive to molecular self-association. Interestingly these two parameters can be directly estimated from ^{15}N relaxation and Diffusion-Ordered Spectroscopy (DOSY) NMR techniques. Therefore we used both of them to demonstrate that Y-FAST exists as a monomer in the apo- or HBR-bound states.

We first predicted the hydrodynamic properties of a monomer of Y-FAST in solution. In absence of high-resolution structure for Y-FAST, we used PYP as a template (~ 94% sequence identity, PDB Code 2PHY) to generate a 3D structural model of Y-FAST using the SWISS-MODEL server. The hydrodynamic properties of the monomeric Y-FAST were predicted using the structural model and the HydroNMR software (3). The viscosity of water surrounding protein was assumed to be similar to water viscosity in the buffer and was predicted using the Sednterp approach (http://sednterp.unh.edu/) (see **Table S4**). The atomic elements radius was set to 3.1 Å. The averaged correlation times predicted at 278 K and 293 K are reported in **Table S4**. The anisotropy was estimated to 1.1 using the $2D_z/(D_x+D_y)$ relationship and the HydroNMR-derived D_x, D_y, D_z parameters. The small anisotropy suggests the almost spherical nature of the monomeric Y-FAST. We further assumed that HBR binding has no effect on Y-FAST structure and hence considered that the correlation time predicted for a monomeric empty Y-FAST is a good approximation to that of the HBR-containing form.

We next compared HydroNMR predictions with experimentally NMR-derived hydrodynamic parameters. The ^{15}N longitudinal (R_1) and transverse (R_2) relaxation rates report on global and internal protein dynamics. Of interest, the global tumbling correlation time τ_c can be directly obtained from the averaged value of the ^{15}N R_2/R_1 ratio (4) for residues without significant internal dynamics. Here we used R_2 and R_1 relaxation parameters modified to subtract the contribution from high-frequency components of the spectral density (5), as implemented in the ROTDIF algorithm (6). We measured the residue-specific ^{15}N R_1, R_2 and heteronuclear {^{1}H}-^{15}N NOE relaxation parameters at two temperatures, 278 and 293 K, and with or without HBR (1:1 ratio) using classical pulse-sequences. Residues with significant internal dynamics were identified from larger or smaller than averaged ^{15}N R_1 or R_2 relaxation parameters or with {^{1}H}-^{15}N heteronuclear NOE values smaller than 0.7. Those residues were excluded for the calculus of the averaged R_2/R_1 ratio. The relaxation parameters were then

analyzed using the ROTDIF software (6) to extract the averaged correlation times that are reported in **Table S4**. Interestingly, under all tested conditions, the measured correlation time was very similar to the predicted correlation time demonstrating that Y-FAST essentially behaves as a monomer in solution. In particular it is noted that ligand binding has limited effect on the oligomeric state of the protein as judged from the similar τ_c with and without HBR.

It has been shown that the measurement of the translational diffusion coefficient can also be used to detect self-association of protein in solution by NMR using the DOSY approach (7, 8). DOSY spectra were collected on Y-FAST in presence or not of one equivalent of HBR at 278 K and 293 K.

The relatively small anisotropy of the rotational diffusion tensor calculated by HydroNMR and the analysis of the shape of the 3D homology model of Y-FAST show that Y-FAST is better approximated by a sphere than by prolate or oblate ellipsoids. Therefore, to calculate the apparent molecular mass (M) of Y-FAST from the translational diffusion coefficient D measured on the DOSY spectrum we used the Stokes-Einstein equation:

$$D = k_B T / (6\eta\pi r_H) \qquad [20]$$

with the Boltzmann constant k_B, the viscosity η, the temperature T and the protein hydrodynamic radius r_H. The viscosity was calculated using the Sednterp approach (see **Table S4**). The hydrodynamic radius (r_H) of a globular protein is directly related to its size, according to the equation:

$$r_H = 4.75\ N^{0.29}\ (\text{in Å}) \qquad [21]$$

where N is the number of residues in the polypeptide chain (9). Each calculated r_H at the two temperatures and in presence or not of HBR was then converted into average molecular weights assuming an averaged amino acid molecular weight of 110 (**Table S4**). By comparison with the theoretical molecular weight of a monomer of Y-FAST (M_{th} = 13,706 Da, 125 amino acids), an excellent correlation was found between translational diffusion-derived molecular weight and the predicted one. This ensures that Y-FAST behaves as a monomer in solution in presence or not of HBR.

Taken together, these NMR experiments are in excellent agreement with a predominant monomeric state of Y-FAST in solution both unbound or bound to HBR.

Text S3: Behavior of Y-FAST upon pH change.

To evaluate the influence of pH on Y-FAST, we study how pH change affects binding. As HMBR is deprotonated in Y-FAST cavity, the thermodynamic dissociation constant K_D associated to the reaction [1] is actually an *apparent* constant, which depends on the concentration of deprotonated HMBR in solution and therefore on the pH of the solution. In the following part, we derive the relationship between the dissociation constant K_D, the proton concentration H fixed by the medium (here the buffer), and the thermodynamic dissociation constant K_- and K_A associated to the binding of deprotonated HMBR in Y-FAST cavity (reaction [22]) and to HMBR ionization (reaction [23]), respectively.

$$\mathbf{A^-} + \mathbf{B} \quad \rightleftarrows \quad \mathbf{A^-\,B} \qquad [22]$$

$$\mathbf{AH} \quad \rightleftarrows \quad \mathbf{H^+} + \mathbf{A^-} \qquad [23]$$

Note that $\mathbf{A^-}$ and **AH** denote the deprotonated and protonated HMBR. Approximating activities with concentrations, the conservation law for HMBR enables to obtain the equation [24].

$$K_D = \left(1 + \frac{H}{K_A}\right) K_- \qquad [24]$$

When $H >> K_A$, equation [24] becomes

$$K_D \approx \frac{HK_-}{K_A} \qquad [25]$$

from which we finally derive

$$log\ K_D = -\ pH\ +\ log\ K_-\ +\ pK_A \qquad [26]$$

We verified experimentally that, in the biologically-relevant pH range 5.5 – 8, log K_D is linearly dependent on the pH with a slope of –1.02 ± 0.12 (**Fig. S15**). This result showed that the change in K_D in this pH range is only due to the change in the relative concentrations of protonated and unprotonated HMBR, and that consequently Y-FAST folding and structure is stable in this pH range. The conclusion of this study is that Y-FAST labeling is highly robust since Y-FAST:HMBR complex can always be fully formed no matter the pH as long as the HMBR concentration used for labeling is significantly greater than the apparent K_D.

Text S4: Dimensional analysis of the rate of labeling in cells and in zebrafish embryos.

Using the characteristic length l of mammalian cells and zebrafish trunk and the characteristic time τ associated with Y-FAST labeling in these systems, it is possible to approximate an apparent diffusion coefficient D for HMBR in these two diffusive media using the relationship $D \sim l^2/\tau$. Typically, for mammalian cells l = 20 µm (typical cell diameter) and τ = 20 s (observed labeling time), while for zebrafish l = 200 µm (typical diameter of embryo trunk) and τ = 30 min (observed labeling time). Dimensional analysis shows that the apparent diffusion coefficient of HMBR in cells and zebrafish are similar $D_{cell} \sim D_{zebrafish} \sim 20\ \mu m^2.s^{-1}$, showing that HMBR diffuses in zebrafish embryo as easily as in 2D cell culture. This value is furthermore comparable with the diffusion coefficient of fluorescein and GFP in the cytoplasm of mammalian cells estimated to be respectively $\sim 100\ \mu m^2.s^{-1}$ (see Nota bene below) and $\sim 30\ \mu m^2.s^{-1}$ (10, 11), suggesting that HMBR diffusion is little affected by the crossing of cell membranes and is therefore highly cell-permeant.

NB: Fluorescein in water displays a diffusion coefficient of $400\ \mu m^2.s^{-1}$ (12); however, the diffusion coefficient depends on the structure of the fluid: typically, it was shown that the diffusion coefficient of small molecules in the cytoplasm of mammalian cells is four-fold smaller than in water (13).

Text S5: Fluorescence Resonance Energy Transfer experiments

Considering its spectral properties, Y-FAST can be used as a donor in a FRET pair with mCherry. To demonstrate this, we determined the yield of the fluorescence resonance energy transfer of electronic excitation in the fusion protein Y-FAST-mCherry by performing a series of cuvette experiments.

We recorded the absorption and emission (λ_{exc} = 470 nm) spectra of 1.5 µM Y-FAST-mCherry in absence and in presence of 250 nM HMBR* (**SI Appendix Fig. 19a**,**b**). In a second step, we recorded the absorption and the emission (λ_{exc} = 470 nm) spectra of 1.5 µM Y-FAST in the presence of 250 nM HMBR† (**SI Appendix Fig. 19a**,**b**).

Denoting **1**, **2**, and **3** the species Y-FAST-mCherry, HMBR:Y-FAST-mCherry, and HMBR:Y-FAST, and $\varepsilon_i(\lambda_{exc})$ and $I_i(\lambda_{exc},\lambda_{em})$ the molar absorption coefficient at λ_{exc} and the intensity of fluorescence emission at λ_{em} of the species **i**, the yield ϕ_{ET} of the fluorescence resonance energy transfer of electronic excitation has been extracted by two different methods from the results of the described series of experiments (14-16):

- We first extracted ϕ_{ET} from the variation of the fluorescence emission of the donor HMBR:Y-FAST. Hence, we wrote:

$$\phi_{ET} = 1 - \frac{I_2(470,550)}{I_3(470,550)}$$

  and found $\phi_{ET} = 0.5 \pm 0.1$;

- We alternatively extracted ϕ_{ET} from the variation of the fluorescence emission of the acceptor mCherry. Hence, we wrote:

$$\phi_{ET} = \frac{[I_2(470,616) - (I_1(470,616) + I_3(470,616))]}{\left(\frac{\varepsilon_1(470)}{\varepsilon_3(470)} I_1(470,616) - I_3(470,616)\right)}$$

  and found $\phi_{ET} = 0.25 \pm 0.15$. This second derivation is notably less reliable since it propagates errors from a large number of experiments (2).

Once ϕ_{ET} determined, we next extracted an order of magnitude for the average distance *R* between HMBR and the mCherry chromophore from assuming fluorescence resonance energy transfer to be governed by the Förster mechanism (14). Hence we wrote

* Under such conditions, the fraction of HMBR:Y-FAST complex is 93%.
† Under such conditions, the fraction of HMBR:Y-FAST complex is 93%.

$$R = R_0 \left(\frac{1}{\phi_{ET}} - 1\right)^{\frac{1}{6}}$$

where R_0 (in nm) designates the Förster distance defined as

$$R_0 = 0.021\left(\kappa^2 \Phi_3 n^{-4} \int_0^\infty I_3(\lambda)\varepsilon_1(\lambda)\lambda^4 d\lambda\right)^{\frac{1}{6}}$$

where κ^2 is the orientational factor (subsequently taken equal to 2/3 upon assuming the donor and the acceptor to sample all orientations), Φ_3 is the fluorescence quantum yield of HMBR:Y-FAST (Φ_3 = 0.33), n is the average refractive index of the medium in the wavelength range where spectral overlap is significant (n = 1.33), $I_3(\lambda)$ is the normalized fluorescence spectrum of HMBR:Y-FAST so that

$$\int_0^\infty I_3(\lambda) d\lambda = 1,$$

$\varepsilon_1(\lambda)$ is the molar absorption coefficient of Y-FAST-mCherry (in $M^{-1}.cm^{-1}$), and λ is the wavelength (in nm). We found $R = 5 \pm 1$ nm, in good agreement with the distance of the two chromophores in our construct containing Y-FAST (modeled as a sphere of diameter ~ 2 nm), a GSSSENLYFQG linker of length ~ 3 nm (considering ~ 0.3 nm per residue), and mCherry (modeled as a cylinder with a ~ 2 nm diameter and a ~ 4 nm height).

SI Materials and Methods

Chemical Synthesis

Commercially available rhodanine (Alfa Aesar), 3-methylrhodanine (Aldrich), rhodanine-3-acetic acid (Aldrich), 4-hydroxybenzaldehyde (Acros), 2,4-dihydroxybenzaldehyde (Aldrich), 4-hydroxy-2-methoxybenzaldehyde (Fluka), 4-hydroxy-3-methylbenzaldehyde (Acros) were used as starting materials without further purification. Analytical and thin layer chromatography (TLC): Merck silica gel 60 F-254 precoated plates; detection by UV (254 nm). NMR spectra were recorded on a AC Bruker spectrometer at 300 MHz for ^{1}H and 75.5 MHz for ^{13}C; chemical shifts are reported in ppm with protonated solvent as internal reference ^{1}H, CHD_2SOCD_3 in CD_3SOCD_3 2.52 ppm, CHD_2OD in CD_3COD 3.34 ppm; ^{13}C, $^{13}CD_3SOCD_3$ in CD_3SOCD_3 40.4 ppm; Coupling constants *J* in Hz. Mass spectra (chemical ionization and electronic impact with NH_3) were performed by the Service de Spectrométrie de Masse de Chimie ParisTech (France). Microanalyses were performed by the Service de Microanalyses de Gif sur Yvette (France).

(Z)-5-(4-hydroxybenzylidene)-2-thioxo-1,3-thiazolidin-4-one (HBR) (17)

A solution containing rhodanine (202 mg; 1.52 mmol) and 4-hydroxybenzaldehyde (195 mg; 1.60 mmol) in 110 mL of water was stirred at 65-80 °C for 10 days. After cooling to room temperature and standing overnight, the precipitate was filtered through a glass filter. After drying over P_2O_5, **HBR** was obtained as a dark yellow powder (235 mg; 65 %). ^{1}H-NMR (300 MHz, CD_3OD) δ(ppm) 7.57 (s, 1 H), 7.45 (d, *J* = 8.7 Hz, 2 H), 6.94 (d, *J* = 8.7 Hz, 2 H).

(Z)-5-(4-hydroxybenzylidene)-3-methyl-2-thioxothiazolidin-4-one (HBMR) (18)

Same as HBR. 3-Methylrhodanine (200 mg; 1.36 mmol), 4-hydroxybenzaldehyde (174 mg; 1.42 mmol), water (110 mL); stirring at 65 °C for 8 days. **HBMR** was obtained as a yellow powder (286 mg; 84 %). ^{1}H-NMR (300 MHz, DMSO-d6) δ(ppm) 7.76 (s, 1 H), 7.54 (d, *J* = 9.0 Hz, 2 H), 6.95 (d, *J* = 9.0 Hz, 2 H), 3.41 (s, 3 H).

(Z)-2-(5-(4-hydroxybenzylidene)-4-oxo-2-thioxothiazolidin-3-yl)acetic acid (HBAAR) (17)

Same as HBR. Rhodanine-3-acetic acid (202 mg; 1.06 mmol), 4-hydroxybenzaldehyde (136 mg; 1.11 mmol), water (110 mL); stirring at 65 °C for 8 days. **HBAAR** was obtained as a yellow powder (127 mg; 41 %). ^{1}H-NMR (300 MHz, DMSO-d6) δ(ppm) 10.57 (s, 1 H), 7.83 (s, 1 H), 7.58 (d, *J* = 8.7 Hz, 2 H), 6.97 (d, *J* = 8.7 Hz, 2 H), 4.75 (s, 2 H).

(Z)-5-(2,4-Dihydroxybenzylidene)-2-thioxo-1,3-thiazolidin-4-one (DHBR) (17, 19, 20)

Same as HBR. Rhodanine (200 mg; 1.50 mmol), 2,4-dihydroxybenzaldehyde (216 mg; 1.56 mmol), water (110 mL); stirring at 65 °C for 8 days. **DHBR** was obtained as a brown powder (138 mg; 36 %). ^{1}H-NMR (300 MHz, DMSO-d6) δ(ppm) 10.66 (s, 1 H), 10.34 (s, 1 H), 7.82 (s, 1 H), 7.17 (d, *J* = 9.0 Hz, 1 H), 6.44 (d, *J* = 9.0 Hz, 1 H), 6.43 (s, 1 H); ^{13}C-NMR (75.5 MHz, DMSO-d6) δ(ppm) 196.2, 170.1, 162.9, 160.3, 131.6, 128.5, 119.2, 112.3, 109.3, 103.0; Mass spec (CI/NH_3) [M+H^+]: 254.0; Anal calc. for $C_{10}H_7NO_3S_2$, 0.29 H_2O (MW: 253+5; water was present in the ^{1}H-NMR spectrum) C: 46.69 % , H: 2.95 % , N: 5.42 % , S 24.81 %; Found C: 46.72 % , H: 2.80 % , N: 5.45 % , S 26.25 %.

(Z)-5-(4-hydroxy-3-methoxybenzylidene)-2-thioxo-1,3-thiazolidin-4-one (HMOBR)

Same as HBR. Rhodanine (200 mg; 1.50 mmol), 4-hydroxy-2-methoxybenzaldehyde (237 mg; 1.56 mmol), water (140 mL); stirring at 65 °C for 8 days. **HMOBR** was obtained as a dark yellow powder (239 mg; 60 %). ^{1}H-NMR (300 MHz, DMSO-d6) δ(ppm) 10.57 (s, 1 H), 7.77 (s, 1 H), 7.26 (d, *J* = 8.4 Hz, 1 H), 6.57 (dd, *J* = 8.4 Hz and 3.6Hz, 1 H), 6.54 (d, *J* = 3.6 Hz, 1 H), 3.87 (s, 3 H); ^{13}C-NMR (75.5 MHz, DMSO-d6) δ(ppm) 196.3, 170.1, 163.2, 160.9, 132.2, 128.0, 120.8, 113.3, 109.5, 99.9, 56.2; Mass spec (CI/NH_3) [M+H^+] : 268.0; Anal calc. for $C_{11}H_9NO_3S_2$ (MW: 267) C: 49.42 % , H: 3.39 % , N: 5.24 % , S 23.99 %; Found C: 49.15 % , H: 3.47 % , N: 5.30 % , S 24.21 %

(Z)-5-(4-hydroxy-3-methylbenzylidene)-2-thioxo-1,3-thiazolidin-4-one (HMBR) (21)

Same as HBR. Rhodanine (200 mg; 1.50 mmol), 4-hydroxy-3-methylbenzaldehyde (213 mg; 1.56 mmol), water (130 mL); stirring at 65 °C for 8 days. **HMBR** was obtained as a yellow

powder (198 mg; 53 %). ^{1}H-NMR (300 MHz, DMSO-d6) δ(ppm) 10.39 (s, 1 H), 7.54 (s, 1 H), 7.35 (d, *J* = 2.7 Hz, 1 H), 7.33 (dd, *J* = 7.8 Hz and 2.7Hz, 1 H), 6.96 (d, *J* = 7.8 Hz, 1 H), 2.19 (s, 3 H); ^{13}C-NMR (75.5 MHz, DMSO-d6) δ(ppm) 196.1, 170.0, 159.2, 134.1, 133.2, 131.1, 126.0, 124.3, 121.2, 116.1, 16.4; Mass spec (CI/NH_3) [M+H^+] : 252.0; Anal calc. for $C_{11}H_9NO_2S_2$ (MW: 251) C: 52.57 %, H: 3.61 %, N: 5.57 %, S 25.52 %; Found C: 52.68 %, H: 3.64 %, N: 5.58 %, S 25.58 %.

Physico-chemical experiments

pH measurements were performed on a Standard pH meter PHM210 Radiometer Analytical (calibrated with aqueous buffers at pH 4 and 7 or 10) with a Crison 5208 Electrode (Barcelona, Spain). UV/Vis absorption spectra were recorded in 1 cm × 1 cm quartz cuvettes (Hellma) on a diode array UV/Vis spectrophotometer (Evolution array, Thermo Scientific). Corrected fluorescence spectra upon one-photon excitation were recorded with a Photon Technology International QuantaMaster QM-1 spectrofluorimeter (PTI, Monmouth Junction, NJ) equipped with a Peltier cell holder (TLC50, Quantum Northwest, Shoreline, WA). The overall emission quantum yields after one-photon excitation ϕ were calculated from the relation:

$$\phi = \phi_{ref} \frac{1-10^{-A_{ref}(\lambda_{exc})}}{1-10^{-A(\lambda_{exc})}} \frac{D}{D_{ref}} \left(\frac{n}{n_{ref}} \right)^2$$

where the subscript *ref* stands for standard samples, $A(\lambda_{exc})$ is the absorbance at the excitation wavelength λ_{exc}, D is the integrated emission spectrum, and n is the refractive index for the solvent. The uncertainty for the experimental value of ϕ was estimated to be ± 20%. The standard fluorophore for the quantum yield measurements was Fluorescein in sodium hydroxide 0.1 M with ϕ_{ref} = 0.92 (ref. (22)). The titration experiments used for the determination of the thermodynamic constants were performed on a SpectraMax®M5e (Molecular Devices) plate-reader. The on- and off-rate constants were determined by stopped-flow experiments using a RX2000 rapid kinetic stopped flow accessory (Applied Photophysics, Leatherhead, UK). Circular dichroism spectra were recorded on a J-815 CD spectropolarimeter (Jasco).

Plasmid constructions

The gene of *Halorhodospira halophila* PYP-C69G codon-optimized for expression in yeast and the gene of Y-FAST codon-optimized for expression in human cells were synthesized by Eurofins Genomics. The plasmid pAG14 enabling the expressing of PYP-C69G in fusion to Aga2p for expression at the yeast cell surface was obtained by inserting the gene of PYP-C69G[‡] between *Nhe* I and *BamH* I restriction sites in the pCTCON2 vector (from the lab of K.D. Wittrup). The plasmids pAG86, pAG87, pAG88, pAG89, pAG90, pAG91 and pAG95 driving bacterial and in vitro expression of clone 2, clone 3 (= Y-FAST), clone 4, clone 5, clone 6 and PYP-C69G, respectively, with an N-terminal His-tag under the control of a T7 promoter were obtained by inserting the gene encoding ENLYFQG–cloneX[§] (X = 2-6)(or PYP-C69G[‡]) between *Nhe* I and *Xho* I restriction sites in the pET28a vector (the sequence ENLYFQG corresponds to the sequence recognized by the TEV protease, enabling removal of the His-tag by TEV digestion). The plasmid pAG101 for bacterial/in vitro expression of mCherry–Y-FAST under the control of a T7 promoter was obtained by inserting the sequence coding for mCherry–GSSSENLYFQG–Y-FAST[§] between *Nhe* I and *Xho* I restriction sites in the pET28a vector. The plasmids pAG135, pAG136, pAG137 for in vitro expression of UnaG, EGFP, Venus with a N-terminal His-tag under the control of a T7 promoter were obtained by inserting the gene encoding each protein between *Nhe* I and *Xho* I restriction sites in the pET28a vector. The vector pThtBAPluc for the in vitro expression of *Firefly* luciferase under the control of a T7 promoter was constructed similarly as in ref. (23) with Luc coding sequence from pEGFPluc (Clontech). The plasmids pAG96 and pAG97 for the mammalian expression of mCherry fused to Y-FAST or to PYP-C69G were obtained by cloning the sequence encoding mCherry–GGGS–Y-FAST[§](or PYP-C69G[‡]) between *Bgl* II and *Not* I restriction sites in the pIRES vector (Clontech). Likewise, the plasmids pAG29, pAG104, pAG106, pAG110 for the expression of EGFP, Y-FAST, Y-FAST fused to membrane localization signal lyn11 (Lyn11-Y-FAST) and Y-FAST fused to the microtubule-binding protein Ensconsin (Ensconsin-Y-FAST), respectively, were obtained by inserting the sequence encoding EGFP–GGGSGGGSPG, Y-FAST[**]–GSEQKLISEEDL, MGCIKSKGKDSAGGGS–Y-FAST[**]–GSEQKLISEEDL, Ensconsin-SAGGGS–Y-FAST[**]–GSEQKLISEEDL (GSEQKLISEEDL = myc-tag). The plasmids pAG109, pAG156 and pAG157 for the expression of Y-FAST fused to zebrafish H2B (H2B–Y-FAST), Y-FAST

[‡] Sequence codon-optimized for expression in yeast.
[§] Sequence selected by yeast display.
[**] Sequence codon-optimized for expression in human cells.

fused to the mitochondrial targeting sequence (mito) from subunit VIII of human cytochrome c oxidase (mito-Y-FAST), Y-FAST fused to N-terminal 81 amino acids of the human beta-1,4-galactosyltransferase for Golgi targeting (golgi-Y-FAST), respectively, were obtained by inserting the sequences encoding H2B–Y-FAST[**]–GSEQKLISEEDL, mito–Y-FAST[**]–GSEQKLISEEDL and golgi–Y-FAST[**]–GSEQKLISEEDL between *Nhe* I and *Not* I restriction sites in the pIRES vector. The plasmids pAG113 and pAG114 for the synthesis of the mRNA encoding mCherry–P2A–Y-FAST and mCherry–P2A–PYP-C69G for zebrafish injection were obtained by inserting the coding sequence for mCherry-GSG ATNFSLLKQAGDVEENPGPSRGGGS–Y-FAST[§] (or PYP-C69G[‡]) between *BamH* I and *SnaB* I in a modified version of pCS2. The plasmids driving the expression of Y-FAST-Gephyrin and Cerulean-Gephyrin were obtained by fusion of the coding sequences of Y-FAST[**] or monomeric Cerulean (containing the A206K point mutation (24)) to the N-terminus of rat gephyrin (GenBank X66366, splice variant P1) via a GGSLGG linker peptide, and insertion into the lentivirus replicon plasmid pFUGW(25) at the restriction sites *Xba* I and *EcoR* I. The plasmid UnaG/pcDNA3-FLAG (26) for the mammalian expression of UnaG was a kind gift of A. Miyawaki. All sequences were verified by DNA sequencing.

Gene encoding PYP-C69G *codon-optimized for expression in yeast cells*

```
ATGGAACATGTTGCCTTTGGTAGCGAAGATATCGAGAATACTCTAGCGAAAATGGATGATGGCCAATTAGATGGA
TTAGCCTTTGGTGCTATACAGCTTGATGGTGATGGCAATATTCTGCAGTATAATGCAGCTGAAGGAGACATAACA
GGGAGAGATCCCAAACAAGTGATTGGCAAGAACTTCTTCAAAGACGTAGCACCAGGTACAGATTCTCCTGAATTT
TACGGGAAATTCAAGGAAGGAGTAGCATCAGGTAACTTGAATACCATGTTCGAGTATACGTTTGACTACCAAATG
ACTCCAACCAAGGTTAAAGTCCACATGAAGAAGGCTTTGAGTGGTGACTCCTATTGGGTGTTTGTCAAAAGGGT
```

Gene encoding Y-FAST *selected by yeast display*

```
ATGGAACATGTTGCCTTTGGTAGCGAAGATATCGAGAATACTCTAGCGAAAATGGATGATGGCCAATTAGATGGA
TTAGCCTTTGGTGCTATACAGCTTGATGGTGATGGCAATATTCTGCAGTATAATGCAGCTGAAGGAGACATAACA
GGGAGAGATCCCAAACAAGTGATTGGCAAGAACTTCTTCAAAGACGTAGCACCAGGTACAGATTCTCCTGAATTT
TACGGGAAATTCAAGGAAGGAGTAGCATCAGGTAACTTGAATACCATGTTCGAGTGGATGATTCCGACGAGTAGG
GGGCCAACCAAGGTTAAAGTCCACATGAAGAAGGCTTTGAGTGGTGACTCCTATTGGGTGTTTGTCAAAAGGGTT
```

Gene encoding Y-FAST *codon-optimized for expression in human cells*

```
ATGGAGCATGTTGCCTTTGGCAGTGAGGACATCGAGAACACTCTGGCCAAAATGGACGACGGACAACTGGATGGG
TTGGCCTTTGGCGCAATTCAGCTCGATGGTGACGGGAATATCCTGCAGTACAATGCTGCTGAAGGAGACATCACA
GGCAGAGATCCCAAACAGGTGATTGGGAAGAACTTCTTCAAGGATGTTGCACCTGGAACGGATTCTCCCGAGTTT
TACGGCAAATTCAAGGAAGGCGTAGCGTCAGGGAATCTGAACACCATGTTCGAATGGATGATACCGACAAGCAGG
GGACCAACCAAGGTCAAGGTGCACATGAAGAAAGCCCTTTCCGGTGACAGCTATTGGGTCTTTGTGAAACGGGTG
```

PYP-C69G protein sequence

```
MEHVAFGSEDIENTLAKMDDGQLDGLAFGAIQLDGDGNILQYNAAEGDITGRDPKQVIGKNFFKDVAPGTDSPEF
YGKFKEGVASGNLNTMFEYTFDYQMTPTKVKVHMKKALSGDSYWVFVKRV
```

Y-FAST protein sequence

```
MEHVAFGSEDIENTLAKMDDGQLDGLAFGAIQLDGDGNILQYNAAEGDITGRDPKQVIGKNFFKDVAPGTDSPEF
YGKFKEGVASGNLNTMFEWMIPTSRGPTKVKVHMKKALSGDSYWVFVKRV
```

Yeast display

Library construction. The yeast display libraries were constructed from the gene of PYP-C69G‡ by saturation mutagenesis using NNK degenerated primers. Library 1 randomized at positions 52, 53, 65, 66, 67, 68, 69 was constructed as followed: two PCR fragments were generated using the pairs of primers AG42/AG43 and AG44/AG46, then assembled by PCR using AG42/AG46 (primers are listed below). The PCR product was digested with *Nhe* I and *BamH* I, and then ligated in pCTCON2 using *Nhe* I / *BamH* I restriction sites. Large-scale transformation performed by electroporation in DH10B *E. coli* cells led to 7×10^7 transformants. DNA was then minipreped, and retransformed in EBY100 yeast strain using large-scale high-efficiency transformation protocol (27), leading to 8×10^7 transformants. Library 2 randomized at 94, 95, 96, 97, 98, 99, 100, 101 was constructed as followed: a PCR product was generated using the pair of primers AG42/AG45. The PCR product was digested with *Nhe* I and *Sty* I, and then ligated in pAG14 using *Nhe* I / *Sty* I restriction sites. Large-scale transformation performed by electroporation in DH10B *E. coli* cells led to 3×10^7 transformants. DNA was purified, and retransformed in EBY100 yeast strain using a large-scale high-efficiency transformation protocol (27), leading to 8×10^6 transformants. Library 3 randomized at 52, 53, 65, 66, 67, 68, 69, 94, 95, 96, 97, 98, 99, 100, 101 was constructed as followed: two PCR fragments were generated using the pairs of primers AG42/AG43 and AG44/AG45, then assembled by PCR using AG42/AG45. The PCR product was digested with *Nhe* I and *Sty* I, and then ligated in pAG14 using *Nhe* I / *Sty* I restriction sites. Large-scale transformation performed by electroporation in DH10B *E. coli* cells led to 1.5×10^7 transformants. DNA was purified and retransformed in EBY100 yeast strain using large-scale high-efficiency transformation protocol (27), leading to 8×10^7 transformants.

AG42: 5′-GGTCGGCTAGCATGGAACATG-3′

AG43: 5′-AAGTTCTTGCCAATCACTTGTTTGGGMNNMNNCCCTGTTATGTCTCCTTC-3′

AG44: 5′-GATTGGCAAGAACTTCTTCAAANNKNNKNNKNNKNNKACAGATTCTCCTGAATTTTAC-3′

AG45: 5′-TTTAACCTTGGTTGGMNNMNNMNNMNNMNNMNNMNNMNNCTCGAACATGGTATTCAAG-3′

AG46: 5′-TTTGTTCGGATCCAACCCTTTTG-3′

AG47: 5′-CGTTCCAGACTACGCTCTGC-3′

Selection. Libraries (typically 1×10^{10} cells) were grown overnight (30°C, 280 rpm) in 1 L of SD (20 g/L dextrose, 6.7 g/L yeast nitrogen base, 1.92 g/L yeast synthetic dropout without tryptophane, 7.44 g/L NaH_2PO_4 and 10.2 g/L Na_2HPO_4-$7H_2O$, 1% penicillin-streptomycin

10,000 U/mL). 1×10^{10} cells yeast cells were then collected and grown for 36 h (23°C, 280 rpm) in 1L SG (20 g/L galactose, 2 g/L dextrose, 6.7 g/L yeast nitrogen base, 1.92 g/L yeast synthetic dropout without tryptophane, 7.44 g/L NaH_2PO_4, 10.2 g/L Na_2HPO_4-$7H_2O$, 1% penicillin-streptomycin 10,000 U/mL). 6×10^8 induced cells were then pelleted by centrigugation (25°C, 3 min, 2,500 g), washed with 10 mL DPBS-BSA (137 mM NaCl, 2.7 mM KCl, 4.3 mM Na_2HPO_4, 1.4 mM KH_2PO_4, 1 g/L bovine serum albumin, pH 7.4), and incubated for 30 min at room temperature in 200 µL of 1/250 primary antibody chicken anti-c-Myc IgY (Life Technologies) solution in DPBS-BSA. Cells were then washed with 10 mL DPBS-BSA, and incubated in 200 µL of 1/100 secondary antibody Alexa Fluor® 647–goat anti-rabbit IgG (Life Technologies) solution in DPBS-BSA for 30 min on ice. After washing with DPBS-BSA, cells were incubated in 10 mL DPBS-BSA supplemented with 20 µM HBR, and sorted on a MoFlo™ XDP High-Speed Cell Sorter equipped with a 488 nm and a 633 nm laser. The sorted cells were collected in SD, grown overnight (30°C, 240 rpm) and spread on SD plates (SD supplemented with 182 g/L sorbitol, 15 g/L agar). Plates were incubated for 60 h at 30°C. The cell lawn was collected in SD supplemented with 30% glycerol, aliquoted and frozen or directly used in the next round.

Protein expression, purification and analysis

Expression vectors were transformed in Rosetta(DE3)pLysS *E. coli* (New England Biolabs). Cells were grown at 37°C in Lysogeny Broth (LB) medium complemented with 50 µg/ml kanamycin and 34 µg/ml chloramphenicol to OD_{600nm} 0.6. Expression was induced for 4 h by adding isopropyl β-D-1-thiogalactopyranoside (IPTG) to a final concentration of 1 mM. Cells were harvested by centrifugation (6,000 × g for 15 min at 4°C) and frozen. The cell pellet was resuspended in lysis buffer (phosphate buffer 50 mM, NaCl 150 mM, $MgCl_2$ 2.5 mM, protease inhibitor, DNase, pH 7.4) and sonicated (5 min at 20 % of amplitude). The lysate was incubated for 2 h at 4 °C to allow DNA digestion by DNase. Cellular fragments were removed by centrifugation (15,000 × g for 1h at 4°C). The supernatant was incubated overnight at 4°C under gentle agitation with Ni-NTA agarose beads in phosphate buffered saline (PBS) (sodium phosphate 50 mM, NaCl 150 mM, pH 7.4) complemented with 10 mM Imidazole. Beads were washed with 20 volumes of PBS containing 20 mM Imidazole, and with 5 volumes of PBS complemented with 40 mM Imidazole. His-tagged proteins were eluted with 5 volumes of PBS complemented with 0.5 M Imidazole, followed by dialysis with PBS. The His-tag was cleaved by incubation of the protein sample with His-tagged Tobacco Etch Virus protease (TEV) for 18 h at 18 °C. After removal of the TEV protease using Ni-NTA beads, the protein sample was eventually dialyzed extensively against 2.5 mM sodium phosphate buffer, lyophilized, and stored at 4 °C. For ^{15}N labelling of Y-FAST, cells were grown at 37°C in M9 minimum medium containing $^{15}NH_4Cl$ complemented with 50 µg/ml kanamycin to OD_{600} 0.8. Expression was induced for 24 h by adding IPTG to a final concentration of 1 mM. Analytical size-exclusion chromatography was performed at 16°C on an Äkta Purifier system (GE Healthcare) equipped with a superdex 200 5/150 GL column and calibrated with Dextran blue, Ferritine, Conalbumine, Carbonic Anhydrase, Aldolase, Ovalbumine and Ribonuclease. Pre-equilibration of the column was performed with pH 7.4 PBS (sodium phosphate 50 mM, NaCl 150 mM). The elution flow rate was set at 0.2 ml / min.

NMR spectroscopy experiments

The ^{15}N relaxation NMR experiments were performed on samples composed of 500 µM ^{15}N-labeled Y-FAST with HBR (1:1 ratio) or without in 50 mM sodium phosphate buffer, 150 mM NaCl pH 7.4, 96:4 H_2O/D_2O, 0.2% DMSO. All NMR experiments were collected using a 800 MHz Bruker spectrometer equipped with a TCI cryoprobe. The residue-specific ^{15}N R_1, R_2 and heteronuclear $\{^1H\}$-^{15}N NOE relaxation parameters were measured at two temperatures, 278 and 293 K, and with or without HBR (1:1 ratio) using classical pulse-sequences. Residues with significant internal dynamics were identified from larger or smaller than averaged ^{15}N R_1 or R_2 relaxation parameters or with $\{^1H\}$-^{15}N heteronuclear NOE values smaller than 0.7. Those residues were excluded for the calculus of the averaged R_2/R_1 ratio. The relaxation parameters were then analyzed using the ROTDIF software (6) to extract the averaged correlation times.

DOSY spectra were collected on Y-FAST in presence or not of one equivalent of HBR at 278 K and 293 K, using a 5-mm triple resonance z-gradient probe head which delivers a maximum gradient strength of 5.35 G/cm. The strength of the gradient pulses, of 1.6 msec duration, was incremented from 2 to 95% in 20 experiments, with a diffusion time of 250 msec. A π/2 phase-shifted squared sine bell window function was applied before the Fourier transformation (FT) and a baseline correction was then conducted after the FT.

Toxicity cellular assay

HeLa cells were incubated with HBR and HMBR solutions at the indicated concentrations for various durations. Cell viability was assayed by fluorescence microscopy using The LIVE/DEAD® viability/cytotoxicity assay kit (Molecular Probes, Life Technologies) following the manufacter's protocol.

Cell-free protein synthesis

The cell-free protein synthesis was performed using the PURExpress in vitro Protein Synthesis Kit (New England Biolabs) according to the manufacturer's protocol. Reaction mix was complemented with HMBR, bilirubin (Sigma) and luciferin (Promega) as indicated. Luminescence emissions were followed over time using a SpectraMax®M5e plate-reader (Molecular Devices).

Microfluidics

A rapid prototyping technique has been used for the device fabrication. A digital cutting machine (Graphtec, CE6000) was used to produce a 0.5 mm wide microfluidic channel in a 0.5 mm thick silicone layer, which was supported by a 50 μm thick plastic film. After removing the plastic film and oxygen plasma treatment, the silicone layer was bonded to a 5 mm thick layer of polydimethylsiloxane (PDMS) which was prepared by casting a mixture of A and B components of RTV 615 (GE, France) at a 10:1 w/w ratio on a flat silicon wafer and curing it at 80°C for 2h. Then, inlet and outlet holes were punched with a metal tube for connections. Afterward, the silicone-PDMS complex was bonded to a 160 μm thick cover slide after oxygen plasma treatment. Finally, the whole device was put in a 80°C oven for 10 min. Before cell seeding, the device was sterilized under UV exposure for more than 30 min. A solution of fibronectin at 50 μg/ml concentration in 0.1 M $NaHCO_3$ (pH 8) was injected into the channel and incubated at 37 °C for 30 min. The channel was washed three times with PBS solution, then 200 μL cell suspension with a cell density of 100,000 cells/ml was introduced in the device and the whole system was incubated at 37°C for 1 h. Dynamic control of the cellular staining-imaging processes was achieved with a multifunctional fluidic controller (FC-PVL-II, MesoBioSystem). The alternative injection of normal and HMBR-containing culture medium into the microfluidic channel was controlled with a home-made project downloaded to the controller so that the whole staining-imaging processes could be performed in an automatic way.

SI References

1. Coch-Frugoni JA (1957) Tampone universale di Britton e Robinson a forza ionica constante. *Gazz Chem Ital* 87:403–407.

2. Bourdoncle A, et al. (2006) Quadruplex-based molecular beacons as tunable DNA probes. *J Am Chem Soc* 128(34):11094–11105.

3. García de la Torre J, Huertas ML, Carrasco B (2000) HYDRONMR: prediction of NMR relaxation of globular proteins from atomic-level structures and hydrodynamic calculations. *J Magn Reson* 147(1):138–146.

4. Blake-Hall J, Walker O, Fushman D (2004) Characterization of the overall rotational diffusion of a protein from 15N relaxation measurements and hydrodynamic calculations. *Methods Mol Biol* 278:139–160.

5. Fushman D, Cowburn D (2001) Nuclear magnetic resonance relaxation in determination of residue-specific ^{15}N chemical shift tensors in proteins in solution: protein dynamics, structure, and applications of transverse relaxation optimized spectroscopy. *Meth Enzymol* 339:109–126.

6. Walker O, Varadan R, Fushman D (2004) Efficient and accurate determination of the overall rotational diffusion tensor of a molecule from ^{15}N relaxation data using computer program ROTDIF. *J Magn Reson* 168(2):336–345.

7. Morris KF, Johnson CS Jr (1992) Diffusion-ordered two-dimensional nuclear magnetic resonance spectroscopy. *J Am Chem Soc* 114(8):3139–3141.

8. Johnson CS (1999) Diffusion ordered nuclear magnetic resonance spectroscopy: principles and applications. *Prog Nucl Magn Reson Spectrosc* 34(3-4):203–256.

9. Wilkins DK, et al. (1999) Hydrodynamic radii of native and denatured proteins measured by pulse field gradient NMR techniques. *Biochemistry* 38(50):16424–16431.

10. Elowitz MB, Surette MG, Wolf PE, Stock J, Leibler S (1997) Photoactivation turns green fluorescent protein red. *Curr Biol* 7(10):809–812.

11. Swaminathan R, Hoang CP, Verkman AS (1997) Photobleaching recovery and anisotropy decay of green fluorescent protein GFP-S65T in solution and cells: cytoplasmic viscosity probed by green fluorescent protein translational and rotational diffusion. *Biophys J* 72(4):1900–1907.

12. Petrášek Z, Schwille P (2008) Precise Measurement of Diffusion Coefficients using Scanning Fluorescence Correlation Spectroscopy. *Biophys J* 94(4):1437–1448.

13. Verkman AS (2002) Solute and macromolecule diffusion in cellular aqueous compartments. *Trends Biochem Sci* 27(1):27–33.

14. Valeur B, Berberan-Santos MN (2012) Molecular fluorescence: principles and

applications.

15. Piston DW, Kremers G-J (2007) Fluorescent protein FRET: the good, the bad and the ugly. *Trends Biochem Sci* 32(9):407–414.

16. Jares-Erijman EA, Jovin TM (2006) Imaging molecular interactions in living cells by FRET microscopy. *Curr Opin Chem Biol* 10(5):409–416.

17. Zhou J-F, Song Y-Z, Zhu F-X, Zhu Y-L (2006) Facile Synthesis of 5-Benzylidene Rhodamine Derivatives under Microwave Irradiation. *Synth Commun* 36:3297–3303.

18. Russell AJ, et al. (2009) Selective small molecule inhibitors of the potential breast cancer marker, human arylamine N-acetyltransferase 1, and its murine homologue, mouse arylamine N-acetyltransferase 2. *Bioorg Med Chem* 17(2):905–918.

19. Tomašić T, et al. (2010) 5-Benzylidenethiazolidin-4-ones as Multitarget Inhibitors of Bacterial Mur Ligases. *ChemMedChem* 5(2):286–295.

20. Opletalova VV, et al. (2010) Synthesis and characterization of (Z)-5-arylmethylidene-rhodanines with photosynthesis-inhibiting properties. *Molecules* 16(6):5207–5227.

21. Pinson J-A, et al. (2011) Thiazolidinedione-Based PI3Kα Inhibitors: An Analysis of Biochemical and Virtual Screening Methods. *Chemmedchem* 6(3):514–522.

22. Crosby GA, Demas JN (1971) Measurement of photoluminescence quantum yields. Review. *J Phys Chem* (75):991–1024.

23. Nakamura M, et al. (2006) Cell-surface-localized ATP detection with immobilized firefly luciferase. *Anal Biochem* 352(1):61–67.

24. Zacharias DA (2002) Partitioning of Lipid-Modified Monomeric GFPs into Membrane Microdomains of Live Cells. *Science* 296(5569):913–916.

25. Lois C, Hong EJ, Pease S, Brown EJ, Baltimore D (2002) Germline transmission and tissue-specific expression of transgenes delivered by lentiviral vectors. *Science* 295(5556):868–872.

26. Kumagai A, et al. (2013) A Bilirubin-Inducible Fluorescent Protein from Eel Muscle. *Cell* 153(7):1602–1611.

27. Gietz RD, Schiestl RH (2007) Large-scale high-efficiency yeast transformation using the LiAc/SS carrier DNA/PEG method. *Nat Protoc* 2(1):38–41.